Icarus 000 (2017) 1–18

Contents lists available at ScienceDirect

Icarus

journal homepage: www.elsevier.com/locate/icarus

Mineralogical analysis of the Ac-H-6 Haulani quadrangle of the dwarf planet Ceres

F. Tosi[a,*], F.G. Carrozzo[a], F. Zambon[a], M. Ciarniello[a], A. Frigeri[a], J.-Ph. Combe[b], M.C. De Sanctis[a], M. Hoffmann[c], A. Longobardo[a], A. Nathues[c], A. Raponi[a], G. Thangjam[c], E. Ammannito[d], K. Krohn[e], L.A. McFadden[f], E. Palomba[a], C.M. Pieters[g], K. Stephan[e], C.A. Raymond[h], C.T. Russell[i], the Dawn Science Team

[a] *INAF-IAPS Istituto di Astrofisica e Planetologia Spaziali, Via del Fosso del Cavaliere, 100, I-00133 Rome, Italy*
[b] *Bear Fight Institute, 22, Fiddler's Road, P.O. Box 667, Winthrop, WA 98862, USA*
[c] *Max Planck Institute for Solar System Research, Justus-von-Liebig-Weg 3, d-37077 Göttingen, Germany*
[d] *Italian Space Agency (ASI), Via del Politecnico snc, I-00133 Rome, Italy*
[e] *Institute of Planetary Research, German Aerospace Center (DLR), Rutherfordstrasse 2, d-12489 Berlin, Germany*
[f] *NASA/Goddard Space Flight Center, Greenbelt, 8800 Greenbelt Road, MD 20771, USA*
[g] *Department of Earth, Environmental and Planetary Sciences, Brown University, 324 Brook Street, Providence, RI 02912, USA*
[h] *NASA/Jet Propulsion Laboratory and California Institute of Technology, 4800 Oak Grove Drive, Pasadena, CA 91109, USA*
[i] *Institute of Geophysics and Planetary Physics, University of California at Los Angeles, 3845 Slichter Hall, 603 Charles E. Young Drive, East, Los Angeles, CA 90095-1567, USA*

ARTICLE INFO

Article history:
Received 29 April 2017
Revised 4 August 2017
Accepted 9 August 2017
Available online xxx

Keywords:
Asteroids surfaces
Asteroid Ceres
Spectrophotometry
Infrared observations

ABSTRACT

Ac-H-6 'Haulani' is one of five quadrangles that cover the equatorial region of the dwarf planet Ceres. This quadrangle is notable for the broad, spectrally distinct ejecta that originate from the crater Haulani, which gives the name to the quadrangle. These ejecta exhibit one of the most negative ('bluest') visible to near infrared spectral slope observed across the entire body and have distinct color properties as seen in multispectral composite images. Besides Haulani, here we investigate a broader area that includes other surface features of interest, with an emphasis on mineralogy as inferred from data obtained by Dawn's Visible InfraRed mapping spectrometer (VIR), combined with multispectral image products from the Dawn Framing Camera (FC) so as to enable a clear correlation with specific geologic features.

Our analysis shows that crater Haulani stands out compared to other surface features of the quadrangle. Albedo maps obtained in the near infrared range at 1.2 μm and 1.9 μm reveal that the floor and ejecta of Haulani are indeed a patchwork of bright and dark material units. Visible to near-infrared spectral slopes display negative values in crater Haulani's floor and ejecta, highlighting bluish, younger terrains. Diagnostic spectral features centered at ~2.7 μm and ~3.1 μm respectively indicate a substantial decrease in the abundances of magnesium-bearing phyllosilicates and ammoniated phyllosilicates in crater Haulani's floor and bright ejecta. Similar, but less prominent, spectral behavior is observed in other geologic features of this quadrangle, while the general trend in quadrangle Ac-H-6 for these two mineral species is to increase from the northwest to the southeast. However, it is worth noting that the correlation between the ~2.7 μm and ~3.1 μm spectral parameters is generally strong in the Haulani crater's area, but much weaker elsewhere, which indicates a variable degree of mixing between these two major mineral phases in moving away from the crater. Finally, the region of crater Haulani displays a distinct thermal signature and a local enhancement in calcium and possibly sodium carbonate minerals, which is hardly found in the rest of the quadrangle and is likely the result of intense hydrothermal processes following the impact event. These evidences all together confirm the young age of crater Haulani, as they have not been erased or made elusive by space weathering processes.

1. Introduction

At about 940 km in mean diameter, the dwarf planet Ceres is the largest and most massive object in the main asteroid belt. Its

* Corresponding author.
E-mail address: federico.tosi@iaps.inaf.it (F. Tosi).

http://dx.doi.org/10.1016/j.icarus.2017.08.012
0019-1035/

low bulk density, 2162 ± 8 kg/m^3 (Russell et al., 2016; Park et al., 2016), is closer to that of icy satellites than of rocky bodies, and reveals that its interior must contain a substantial amount of water. Morphological analysis of impact craters suggests that this water is likely concentrated in the mantle rather than in the outer crust. Exposed water ice, which on Ceres is thermodynamically unstable at low latitudes (Titus, 2015), has been identified only in a few places, favored by the local topography (Combe et al., 2016; Platz et al., 2016; Nathues et al., 2017; Combe et al., 2017a, this issue; Stephan et al., 2017b, this issue).

The Haulani quadrangle (Ac-H-6) is one out of five that cover the equatorial region of Ceres (Lon 0°–72°E, Lat 22°S to 22°N, Roatsch et al., 2016b). It is named after *Haulani* (Lon 10.77°E, Lat 5.8°N), the fourth largest impact crater (diameter 34 km) in this quadrangle. Other impact craters with an official designation by the International Astronomical Union (IAU) and diameters in the range 20–50 km are: *Anura* (37 km), *Kondos* (44 km), *Piuku* (31 km), *Shakaema* (47 km), and *Tahu* (25 km).

A thorough geologic mapping of this region (Krohn et al., 2017) established that cratered terrain (*crt*) is the oldest and broadest unit in quadrangle Ac-H-6 (and more generally on Ceres), displaying a high crater density, an intermediate albedo (average value 0.03) in FC clear filter images, and a brownish color in enhanced FC color composite images. The second broadest geologic type is crater material, which surrounds well-defined craters except Haulani, and can be further divided into three units: crater material (*c*), bright crater material (*cb*), and dark crater material (*cd*). Crater Haulani is a distinct geologic unit in itself, as it appears to be one of the freshest and youngest surface features on Ceres, being made up by a complex patchwork of subunits of varying extent. It exhibits interior smooth plains with flow features originating from a hummocky elongated mountainous ridge in the center, ponding toward mass-wasting deposits of the rim. Several flow features are observed running from the crater rim outward to the surrounding area, covering the preexisting surface (Krohn et al., 2016). The smooth crater floor is laced by pits. Some pit crater chains in the northwestern part are oriented parallel to the rim (Krohn et al., 2016; Sizemore et al., 2017). Most notable geologic units mapped within crater Haulani are: bright lobate material (*lb*), knobby bright lobate material (*lkb*), smooth lobate material (*ls*), and smooth bright lobate material (*lsb*). Haulani's bright ejecta (*crb*) is widespread over the cerean surface, preferentially to the west, extending into quadrangle Ac-H-10 'Rongo' (Platz et al., 2017; Zambon et al., 2017b, this issue).

Crater Haulani was formed on the transition between a central plateau in the east and a topographic low in the west (Krohn et al., 2016; Krohn et al., 2017). Adjacent to the west of Haulani there is one named domical mountain: *Dalien Tholus* (length: ~22 km, width: ~14 km). *Wangala Tholus*, located in the southwest, is much larger (length: ~50 km) and is cut almost equally by the boundary between the Haulani and Sintana quadrangles (Schulzeck et al., 2017).

Magnesium- and ammonium-bearing phyllosilicates, carbonates and a spectrally featureless dark endmember yet to be identified, are the major surface minerals on Ceres (De Sanctis et al., 2015) and are ubiquitous at 1-km spatial resolution (Ammannito et al., 2016). Ammonia, accreted either as organic matter or as ice, may have reacted with phyllosilicates on Ceres during differentiation, leading to widespread existence of ammoniated phyllosilicates (De Sanctis et al., 2015). Variations in the strength of their diagnostic absorption features may be spatially correlated and indicate considerable variability in the relative abundance of the phyllosilicates, although their composition is fairly uniform. These data, along with the distinctive spectral properties of Ceres relative to other asteroids and carbonaceous meteorites, indicate that the phyllosilicates were formed endogenously by a globally widespread and extensive alteration process (Ammannito et al., 2016).

Besides these two mineral phases, which dominate the surface of Ceres at global scale, in high-albedo areas the relative proportions of the components changes, with a clear increase in carbonate content with respect to the dark material. Cerealia Facula, i.e. the bright unit in the middle of the 92-km crater Occator (in quadrangle Ac-H-9 'Occator'), is especially rich in anhydrous sodium carbonate, and it appears to represent the most concentrated known occurrence of km-scale carbonates beyond the Earth (De Sanctis et al., 2016). The northern flanks of Ahuna Mons, the highest mountain on Ceres (located in quadrangle Ac-H-10 'Rongo'), also display a larger amount of Mg-Ca carbonates and Na-carbonates compared to surrounding regions (Zambon et al., 2017a; Longobardo et al., 2017, this issue).

Water ice-rich units were discovered only in about ten specific places at the surface. The very first detection occurred in the geologically young 10-km Oxo crater, where the relatively high latitude (~42°N) and morphology protects much of the surface area from direct solar illumination for most of the cerean day (Combe et al., 2016). Other occurrences of water ice-rich units mixed with low-albedo components were later discovered at latitudes poleward of ~30° in fresh craters near rim shadows (Combe et al., 2017a, this issue; Stephan et al., 2017b, this issue) and at some permanently shadowed craters (Platz et al., 2016). Furthermore, aliphatic organic matter was found to be mainly localized on a broad region of ~1000 km^2 close to the ~50-km Ernutet crater (De Sanctis et al., 2017a). However, since water ice and organics are not widespread on the Ceres surface but only occur in specific regions of interest outside the Haulani quadrangle, our analysis will use a subset of spectral parameters that are meaningful for this and other quadrangles, consistent with the same approach adopted for other papers found in this special issue.

Here we present a detailed mineralogic study of the Ac-H-6 Haulani quadrangle, similar to what was previously done for the *Av*-10 Oppia quadrangle on Vesta (Tosi et al., 2015b). Most of our mineralogical analysis relies on the latest calibrated near infrared spectra acquired by the Visible and InfraRed mapping spectrometer (VIR) onboard Dawn. The combination of VIR data with imagery acquired by the Framing Camera (FC), showing a higher spatial resolution, enables accurate correlation of spectral units with geologic units and topography. In addition, we also take advantage of the thermal infrared range measured by VIR to derive a spatially-resolved temperature map of Ac-H-6. This unprecedented mineralogic mapping allows for a broader understanding of the processes that gave rise to the currently observed composition, and a better correlation with processes that are found in other quadrangles on Ceres.

2. Data

Launched on 27 September 2007, the Dawn spacecraft closely explored the giant asteroid Vesta from 16 July 2011 to 5 September 2012. After a 2.5-years transfer period, Dawn entered orbit around Ceres on 6 March 2015, following a polar trajectory (Russell et al., 2016).

The data used in this paper have been obtained by the two remote sensing instruments onboard Dawn: VIR and FC. The VIR instrument (De Sanctis et al., 2011) is an imaging spectrometer with an overall spectral range from 0.25 to 5.1 µm, designed to determine the mineral composition of surface materials in their geologic context, and to derive spatially-resolved thermal maps of the surface of the object on its dayside in locations with surface temperatures above ~180 K (Tosi et al., 2014). The FC (Sierks et al., 2011) has a broadband clear filter and seven narrow-band filters (0.4–1.0 µm) that obtained near-global coverage of the surface

Please cite this article as: F. Tosi et al., Mineralogical analysis of the Ac-H-6 Haulani quadrangle of the dwarf planet Ceres, Icarus (2017), http://dx.doi.org/10.1016/j.icarus.2017.08.012

Table 1
Summary of the main observation circumstances for the different Dawn mission phases at Ceres. Different columns are labeled according to the mission phase name or acronym. Different rows respectively report: start date, stop date, mean altitude of the spacecraft above the surface (km), VIR pixel resolution (km), FC pixel resolution (km), and range of phase angle values (degrees).

	Survey	HAMO	LAMO	XMO1	XMO2	XMO3	XMO4
Start date	5 Jun 2015	18 Aug 2015	16 Dec 2015	19 Jun 2016	10 Oct 2016	21 Jan 2017	29 Apr 2017
Stop date	30 Jun 2015	22 Oct 2015	18 Jun 2016	2 Sep 2016	4 Nov 2016	17 Feb 2017	24 May 2017
Mean altitude (km)	4413	1512	378	378	1522	7738	19,457
VIR pixel resolution (km)	1.10	0.38	0.095	0.095	0.38	1.93	4.86
FC pixel resolution (km)	0.41	0.14	0.035	0.035	0.14	0.73	1.82
Phase angle range (deg)	12.4–84.6	23.0–57.5	35.9–80.7	35.9–80.7	58.9–80.0	75.5–84.1	0.0–6.5

revealing detailed albedo and color variations. FC has an angular (pixel) resolution ∼2.67 times better than VIR. FC images have also been used to derive an accurate shape model of the dwarf planet (Preusker et al., 2016).

The orbital mission at Ceres was divided in a number of phases: Survey, High-Altitude Mapping Orbit (HAMO), Low-Altitude Mapping Orbit (LAMO), Extended Low-Altitude Mapping Orbit (XMO1), Extended Juling Orbit (XMO2), Extended Grand Orbit (XMO3), and Ceres Opposition (XMO4). Each phase had a different length and was carried out from a different altitude, with spatial resolution depending on the altitude over the mean surface. Table 1 summarizes the main observational circumstances for these mission phases. In general, the altitude decreased from Survey to LAMO, and then increased again from XMO1 to XMO4.

The different stages of the Dawn mission at Ceres occurred under changing illumination conditions. In a polar orbit, the solar phase angle varies continuously, but the value measured at equatorial sub-spacecraft points' latitudes increased overall from Survey to XMO3, along with a variable coverage of the surface. The most favorable circumstances in terms of coverage, spatial resolution and illumination conditions for spectroscopy were achieved in the Survey phase, even though the spatial resolution was relatively low compared to the subsequent HAMO, LAMO and XMO1 stages. The most limited spatial coverage and lowest signal-to-noise ratio (SNR) were obtained in LAMO and XMO1, due to short exposure times, large phase angles generally inducing long shadows in the observed scene, and smearing. This makes VIR data acquired in this period less optimal for use and interpretation on a region as broad as an entire quadrangle of Ceres.

3. Tools and techniques

3.1. Spectral parameters

While the average reflectance spectrum of Ceres lacks distinctive features in the spectral range 1.0–2.5 µm, the thermally corrected wavelength region 2.6–4.2 µm as explored by VIR in the early Survey orbit phase, which lasted from 5 to 30 June 2015 and obtained nearly global hyperspectral coverage at ∼1.1 km/px, displays a broad asymmetric feature, characteristic of H_2O/OH-bearing materials. Within this broad absorption are several distinct absorption bands, centered respectively at 2.72–2.73 µm, 3.05–3.1 µm, 3.3–3.5 µm and 3.95 µm (De Sanctis et al., 2015). The 2.72–2.73 µm feature is distinctive for OH-bearing minerals. This prominent band is best fitted by a mixture including Mg-bearing phyllosilicates such as Mg-serpentine (antigorite) (Ammannito et al., 2016). NH_4-bearing minerals, such as NH_4-serpentines and NH_4-smectites, show clear absorptions at 3.05–3.1 µm and at 3.3 µm (Bishop et al., 2002; Ehlmann et al., 2017), while the 3.95-µm absorption band has been definitively attributed to carbonates (Rivkin et al., 2006; De Sanctis et al., 2015). These lithologies, plus a spectrally bland dark material that is actually the most abundant spectral endmember, are ubiquitous at ∼1 km spatial resolution (Ammannito et al., 2016; Carrozzo et al., 2017a, this issue).

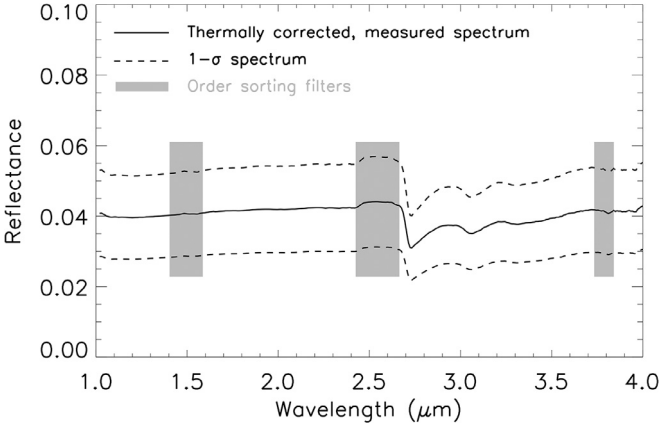

Fig. 1. Average reflectance spectrum of quadrangle Ac-H-6 Haulani in the range 1–4 µm, as measured by VIR in the Survey mission phase (spatial resolution ∼1.1 km/px) under favorable illumination conditions. The spectrum was corrected for the thermal emission (following the approach described in Raponi et al., 2017, this issue) and for the illumination and observation geometry by means of the Hapke model (Ciarniello et al., 2017). The solid line represents the mean spectrum while the dashed lines mark the 1-sigma variability. Gray boxes highlight the spectral counterparts (position and width) of three order sorting filters placed on top of the VIR infrared focal plane, which induce systematic artifacts in VIR spectra.

The identification of the dark endmember is challenging because its spectrum is essentially featureless, except for a tentative absorption band centered at 1 µm, which in principle may be attributed to iron (Fe). While magnetite (Fe_3O_4) provides a good spectral match, a large amount of Fe is inconsistent with GRaND measurements (Prettyman et al., 2017). Since carbonaceous chondrite is the meteoritic analogue closest to the average reflectance spectrum of Ceres (Chapman and Salisbury, 1973), this dark endmember is very likely carbon-bearing material.

Because the 2.7- and 3.1-µm absorbers are observed in all of the geologic units, spanning a broad range of ages and with no correlation between the age and these bands' depths, the corresponding mineral phases are believed to be of endogenous rather than exogenous nature, which means that the outer crust of Ceres is intrinsically enriched in these species.

In Fig. 1 we show an average reflectance spectrum of the A-H-6 Haulani quadrangle in the range 1–4 µm, as measured by VIR in the Survey mission phase, where the main spectral signatures so far described can be identified.

Spectral indices used in this work are: reflectance (measured at given wavelengths), spectral slopes, band center, and band depth. A spectral slope is measured by interpolating the spectral profile between two given wavelengths with a straight line, and computing its angular coefficient. In both the visible and near-infrared spectral ranges, spectral slopes are indicative of the composition, grain size and age of the surface regolith, therefore highlighting both the chemico-physical state and space weathering processes. Band centers (BC) and band depths (BD) are typical spectral parameters

used both in laboratory spectra and in remote sensed spectroscopic datasets to understand the mineralogical composition of a planetary surface and the physical characteristics of the regolith. The band center is the location of the reflectance minimum inside the band after the spectral continuum removal, while the band depth is defined, after Clark and Roush (1984), as: $1\text{-}R_b/R_c$, where R_b and R_c are the reflectance of the band and the spectral continuum at the BC.

The analysis of the band center for the main diagnostic spectral signatures seen in the infrared spectrum of Ceres shows that it does not change significantly for Mg- and NH_4-bearing phyllosilicates, while it can change for carbonate minerals, where an increase in the band center value from 3.95 to 4.01 μm is indicative of a smooth transition between Mg- or (Mg,Ca)-rich carbonates and Na-rich carbonates (e.g., Carrozzo et al., 2017a, this issue; Palomba et al., 2017b, this issue).

Band depths are indicative of a mineral's abundance, the presence of opaque minerals or other phases, and may also depend on the grain size distribution (e.g., Adams, 1974; Clark, 1999). In general, the presence of opaque minerals tends to reduce or even suppress an absorption band, depending on the thickness of the absorbing layer. Unlike band centers, band depth values are affected by illumination and observation geometry, hence a photometric correction is required to allow a proper evaluation of this parameter. In this regard, Ciarniello et al. (2017) applied Hapke's model to the VIR dataset obtained at Ceres in the early mission stages, i.e. Survey and pre-Survey approach phases yielding a spatial resolution >1 km/px, to perform a photometric correction to standard observation geometry (solar incidence angle $i = 30°$, emission angle $e = 0°$, solar phase angle $\alpha = 30°$) at VIS-IR wavelength. This resulted in albedo and color maps of the surface. The same procedure was later applied to HAMO data, in order to also allow proper estimation of band depth values for those datasets, which were used to produce the spectral maps described in the next section.

3.2. Spectral maps

This work is largely based on VIR-derived spectral maps of quadrangle Ac-H-6 Haulani, showing a higher level of detail compared to global spectral maps released previously (Ammannito et al., 2016), and on FC-derived maps of the same region. All maps use the latest products available for these two instruments at the time of writing.

Frigeri et al. (2017, this issue) provide details about how VIR spectral parameters were derived, filtered and mapped. In particular, VIR spectral indices were computed from individual hyperspectral images acquired in the Survey and HAMO phases, and then mosaicked using averaged overlapping values on a grid with a fixed resolution of 140 m/pixel (Frigeri et al., 2017, this issue). This resolution matches the average resolution of FC images obtained in the HAMO phase, to enable a direct comparison between VIR- and FC-derived products. The mineralogical maps of the entire quadrangle, on which our analysis dwells, are based on the band depths of the 2.72–2.73 μm (hereafter 2.7-μm) and 3.05–3.1-μm (hereafter 3.1-μm) spectral features. The composition and abundance of carbonate minerals is evaluated from the gobal maps produced by Carrozzo et al. (2017a, this issue), which have been cut out for quadrangle Ac-H-6. In this case, the carbonate composition is mapped by means of the center of the diagnostic band at ∼4 μm, while its abundance is estimated by computing the depth of the same band. Stripes and spurious values, disconnected from the geologic context, were first removed by using the procedure described in Carrozzo et al. (2016), then each spectrum in units of calibrated radiance factor (I/F) was corrected for thermal emission by removing a Planck function produced by the best fit with the measured spectra (Raponi et al., 2017, this issue), and finally the photometric correction mentioned in the previous section (Ciarniello et al., 2017) was applied to thermally corrected spectra. While few residual artifacts may still show up after this post-processing, further analysis will eventually exclude those values that are not spatially coherent or are clearly the counterpart of spurious instrumental artifacts.

FC color filter data were used to create enhanced color mosaics and a map of spectral slope in the visible to near-infrared range 0.555–0.829 μm. The 'Clementine' color composite map (Pieters et al., 1994) is of interest to evaluate local spectral variations at high spatial resolution, which may trace variations in composition. Comparing Clementine color data and VIR spectral maps is indeed a powerful way to highlight possible correlations between mineralogy and spectrally distinct structures seen in color imagery with higher spatial resolution. On the other hand, while the Clementine color code proved to be optimal for lunar and Vesta data, it may not necessarily be the best presentation to trace compositional differences in other rocky bodies of the Solar System. Therefore, we explored the Haulani region using a second, 'enhanced' color composite map, which is more suited to Ceres, to investigate the existence of spectral textures that would otherwise remain elusive or hidden.

The presence of dark and bright material units can be evaluated by means of albedo or reflectance maps. In our case, we used the following reflectance information: 1) a clear filter FC mosaic obtained during the HAMO phase (∼140 m/pixel), photometrically corrected by applying a phase angle-dependent brightness function (Roatsch et al., 2016b), and 2) two reflectance mosaics derived from VIR data at 1.2 μm and 1.9 μm with a resolution of 140 m/pixel, photometrically corrected using the method described by Ciarniello et al. (2017) and briefly addressed in Section 3.1. Since the 1.2- and 1.9-μm wavelengths in VIR data are unaffected both by known or expected cerean spectral signatures as well as by VIR instrumental artifacts, they turn out to be optimal to sample the spectral continuum in a region dominated by solar reflection. Their use in conjunction with the 2.7-μm and the 3.1-μm BD maps obtained at the same spatial scale is key to highlighting potential correlations arising between reflectance and abundance of Mg- and NH_4-bearing phyllosilicates.

Because the overall mineralogy of Ceres is dominated by these two species, our analysis uses a density scatterplot of band depths at 2.7-μm vs. 3.1-μm, and a map of measured/modeled band depth at 2.7 μm, to highlight those regions that substantially deviate from an ideally linear dependence between these two spectral indices. In addition, we use a four-color map to merge the 2.7-μm and the 3.1-μm BD maps into a single composite map, where colors are indicative of the simultaneous abundance of magnesium-bearing phyllosilicates and ammoniated phyllosilicates.

3.3. Other maps: geologic map, topographic map, temperature map

The availability of the geologic map by Krohn et al. (2017) allows us to associate the composition of the main surface units of the Haulani quadrangle to their relative geologic timescales and therefore achieve a clear picture about the sequence of events that led to the mineralogy that is observed on Ceres today. A digital terrain model (DTM) of the Haulani quadrangle, derived from FC clear-filter data acquired in HAMO with a resolution of 60 pixels/deg or ∼137 m/pixel (Preusker et al., 2016), is also used to cross-check correlations between composition and topography.

The long-wavelength range of VIR sensitivity, 4.5–5.1 μm, is exploited to systematically retrieve surface temperatures. These data were used both to produce global maps and to investigate in detail the behavior of local-scale features (Tosi et al., 2014). The motivation for our investigation is the search for thermal anomalies, i.e. regions whose response to insolation differs from the average

Please cite this article as: F. Tosi et al., Mineralogical analysis of the Ac-H-6 Haulani quadrangle of the dwarf planet Ceres, Icarus (2017), http://dx.doi.org/10.1016/j.icarus.2017.08.012

behavior of the quadrangle and of the dwarf planet as a whole. The surface of Ceres is expected to have a low thermal inertia at global and broadly regional scale (Titus, 2015; Hayne and Aharonson, 2015), but departures from this behavior may be found at the local scale, e.g., due to variations in regolith thickness, density, or thermal conductivity. For this reason, we also included a map of surface temperature of the Ac-H-6 quadrangle derived from VIR infrared data.

In all maps, including the spectral maps described in the previous sub-section, longitudes are given in the Ceres coordinate system (Raymond and Roatsch, 2015). A small crater (~0.4 km diameter) named Kait was chosen by the Dawn Team to define the prime meridian (Roatsch et al., 2016a). The location of this small crater is within the envelope of the broad feature identified in Hubble Space Telescope (HST) data to which the previous system (Archinal et al., 2011) was anchored.

4. General mineralogy of Ac-H-6

4.1. Reflectance, colors and topography from FC data

First, we summarize the main features that have been described in the Haulani quadrangle based on FC data, providing a high-resolution context for subsequent analysis and interpretation of mineralogy data. In this regard, we rely on a comparison between six maps, shown in Fig. 2:a) a reflectance map; b) the geologic map produced by Krohn et al. (2017); c) a Clementine color composite map; d) an 'enhanced' color composite map, alternative to the Clementine color map; e) a map of the spectral slope computed between 0.555 and 0.829 μm; and f) a HAMO-based DTM.

From the FC-derived clear filter reflectance mosaic (Fig. 2a), whose reflectance values range from 0.01 to 0.06, one can infer the existence of bright and dark materials, which stand out as having substantially higher or lower reflectances than the quadrangle's average value of 0.03. In Ac-H-6, most of these dark and bright materials are associated with crater Haulani, which overall is one of the brightest features on Ceres, with its bright interior and its extensive ejecta with far-ranging crater rays (Krohn et al., 2017). The high albedo of the Haulani area was first recognized in Hubble Space Telescope (HST) images (Li et al., 2006) and then relocated in Dawn FC Approach and Survey images (Li et al., 2016).

Geologic mapping of quadrangle Ac-H-6 (Fig. 2b, from Krohn et al., 2017) established that, among bright units found in Haulani, knobby bright lobate material (*lkb*) extends around the northern and eastern crater rim, and smooth bright lobate material (*lsb*) only occurs as smaller branches in the south-southeast and north-northeast, covering the surface with streaky flow-like material. Particularly prominent is a bright lobate material (*lb*), extending westward. This material shows a relatively smooth surface with many flow fronts. Crater floor hummocky bright material (*cfhb*) also occurs only in Haulani crater and shows a high albedo. Finally, bright crater ray material (*crb*) deposits occur as bright streaks or radial halos around the Haulani impact crater and cover the adjacent terrain with a somewhat thin layer. This unit exhibits a high albedo compared to the surrounding terrain in FC clear filter images.

Among dark units, crater floor material dark (*cfd*) has a similar morphology and albedo as the *cf* unit, but in the enhanced FC color images this unit appears dark blue to black. The *cfd* unit was only found in Shakaema crater. The crater floor material smooth dark (*cfsd*) in Haulani contains many pits. Crater dark material (*cd*) is only found at Kondos crater and also covers the crater rim and floor, forming a continuous surface.

The Clementine composite map of quadrangle Ac-H-6 (red: 0.75/0.44 μm, green: 0.75/0.92 μm, blue: 0.44/0.75 μm) (Fig. 2c) shows that most of the surface is reddish, while crater Haulani stands out to be the most prominent multispectral unit, displaying an overall light blue color, with bright crater ray material appearing cyan, dark material appearing bluish/violet, and the brightest units in the crater's floor displaying a greenish color. However, the southeastern inner wall of Haulani, and smaller patches close to the northern rim, which may represent redeposited slumping material from the southern topographic heights (Stephan et al., 2017a), retain the red color typical of the rest of the quadrangle. Besides Haulani, which is by far the most striking feature in this quadrangle, there are other examples of bluish material units highlighted by the Clementine color code: 1) a small unnamed crater located at 13.7°S/11.2°E, roughly in the middle of Anura crater's floor, which excavated fresh material from below, 2) a small unnamed crater centered at 20.7°N/7.6°E, i.e. close to the borderland between Ac-H-6 and Ac-H-2 quadrangles, and 3) the ejecta of two small unnamed craters, centered respectively at 9.9°S/21.0°E and 17.0°N/62.3°E.

To complement the analysis of the Haulani quadrangle based on multispectral FC data, we have used a second color scheme, which is more suited to Ceres (Fig. 2d). In this 'enhanced' color composite mosaic (red: 0.96 μm; green: 0.75 μm; blue: 0.44 μm), most of the surface in quadrangle Ac-H-6 (and more generally on Ceres) displays a brownish color, while crater Haulani remains the most prominent multispectral unit, with ejecta material displaying a typical bluish color. Compared to the Clementine presentation, this color scheme shows many more color shades and enhances differences in albedo, with bright materials concentrated particularly in the Haulani crater's floor, appearing cyan, while dark material units found in the Shakaema and Kondos craters, and to a lesser extent in other craters of smaller size including Haulani itself, appear dark blue to violet. However, subtle differences can be noticed in the southeastern inner wall of Haulani as well as other smaller patches located just below its northern rim, when using this color scheme compared to the Clementine color scheme.

The map of visual spectral slope, calculated between 0.555 and 0.829 μm (Fig. 2e), reveals that the majority of the quadrangle has a greenish and whitish color, indicating a null (flat) or slightly positive slope value. Crater Haulani stands out for its blue/dark blue/red colors corresponding to negative values of spectral slope, especially in its floor and ejecta (Stephan et al., 2017a). In moving away from Haulani, the value of the spectral slope gradually decreases to background levels. Extreme negative values (down to −0.03) are recorded in the middle and western part of the crater's floor, and in the ejecta closer to the rim, while the southeastern inner wall, as well as some minor localized patches in the eastern, northern and north-eastern inner walls close to the rim, display a positive spectral slope. The negative values of spectral slope recorded in the area of crater Haulani are extreme not only within this quadrangle, but more generally on the entire surface of Ceres, other very blue surface features being Oxo and Ahuna Mons, followed by Occator and Kupalo (Schröder et al., 2017).

Across quadrangle Ac-H-6, the 0.555–0.829 μm spectral slope overall increases in moving from west to east, while other exceptions represented by negative values of spectral slope (albeit less prominent than in crater Haulani) are found in a small unnamed crater at 13.7°S/11.2°E, in the floor of crater Anura, and in the ejecta of crater Anura, as well as in other three small unnamed craters, centered respectively at: 20.7°N/7.6°E, 9.9°S/21.0°E, and 17.0°N/62.3°E. Age determinations indicate that the bluish material is mainly associated with the youngest impact craters on Ceres (Nathues et al., 2016; Schmedemann et al., 2016).

Fig. 2f is a portion of the DTM of Ceres for the Ac-H-6 quadrangle, where the color palette reflects the local topography (Preusker et al., 2016). The maximum topographic relief that occurs in this

Please cite this article as: F. Tosi et al., Mineralogical analysis of the Ac-H-6 Haulani quadrangle of the dwarf planet Ceres, Icarus (2017), http://dx.doi.org/10.1016/j.icarus.2017.08.012

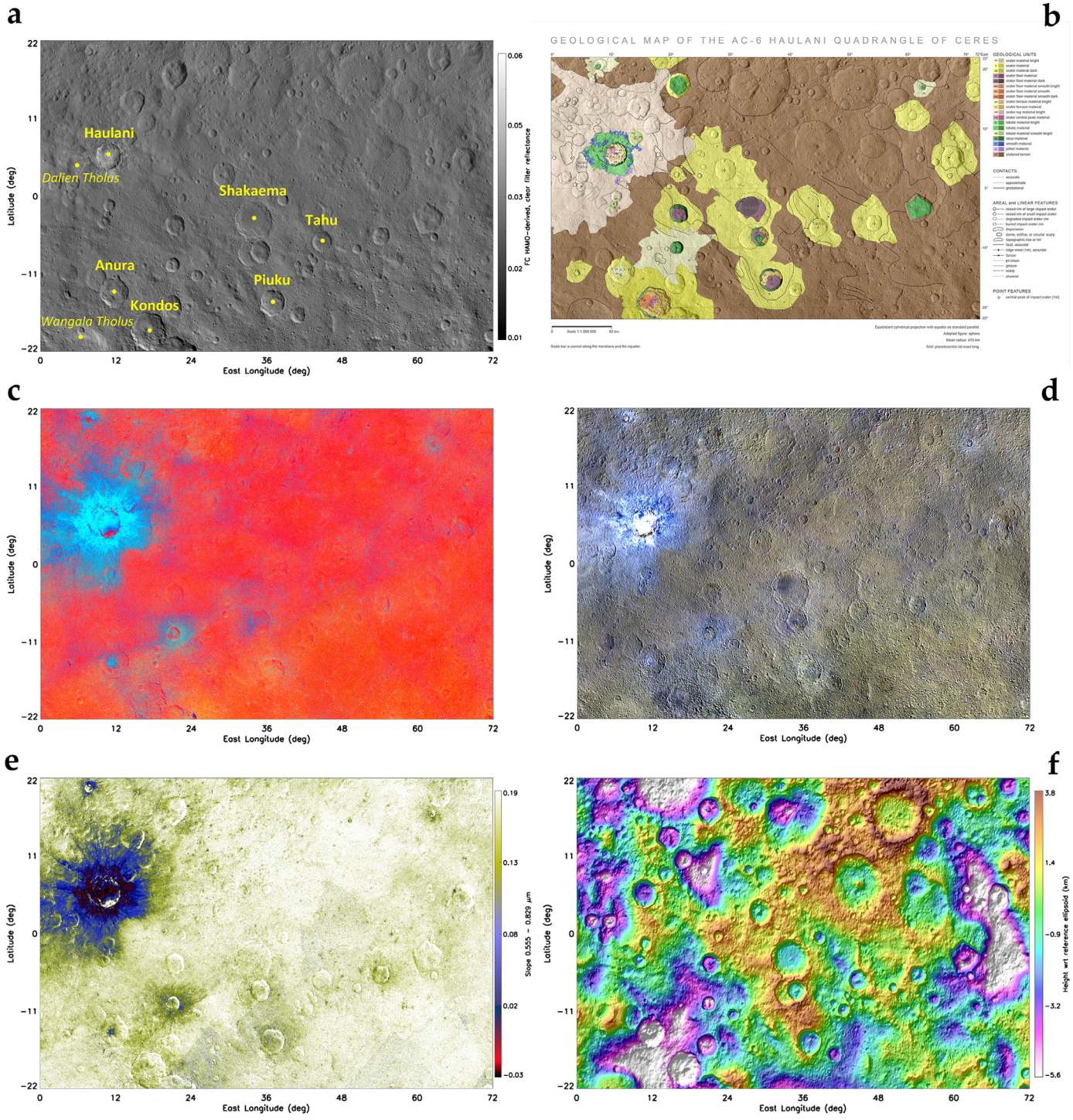

Fig. 2. a: Reflectance map of Ac-H-6 Haulani, obtained through photometric correction of FC clear-filter data acquired in the HAMO mission phase. The map scale is ~140 m/pixel. Surface features that have received an official designation by the IAU are marked in yellow. **b:** Geologic map of Ac-H-6 Haulani, from Krohn et al. (2017). The broad brownish geologic unit is mapped as 'cratered terrain' (*crt*). Yellow patches of 'crater material' (*c*) are found in the vicinity of the main impact craters. **c:** RGB composite of the Ac-H-6 Haulani quadrangle made from FC color ratios: *R*: 0.75/0.44 µm, *G*: 0.75/0.92 µm, *B*: 0.44/0.75 µm ('Clementine' color composite). Color ratios may enhance differences in material and composition. **d:** RGB composite of the Ac-H-6 Haulani quadrangle made from FC colors: *R*: 0.96 µm; *G*: 0.75 µm; *B*: 0.44 µm ('enhanced' color composite). Compared to the Clementine presentation, this color scheme enhances differences in albedo. **e:** RGB composite of the Ac-H-6 Haulani quadrangle showing spectral slope calculated between 0.555 and 0.829 µm. **f:** Portion of the digital terrain model (DTM) derived from FC images acquired in HAMO, at a scale of 60 pixels/degree. The color palette follows height in km with respect to the reference ellipsoid (i.e., the curvature of the body is removed), with the highest elevations in brown and the lowest terrains in magenta/white. (For interpretation of the references to color in this figure legend, the reader is referred to the web version of this article.)

Please cite this article as: F. Tosi et al., Mineralogical analysis of the Ac-H-6 Haulani quadrangle of the dwarf planet Ceres, Icarus (2017), http://dx.doi.org/10.1016/j.icarus.2017.08.012

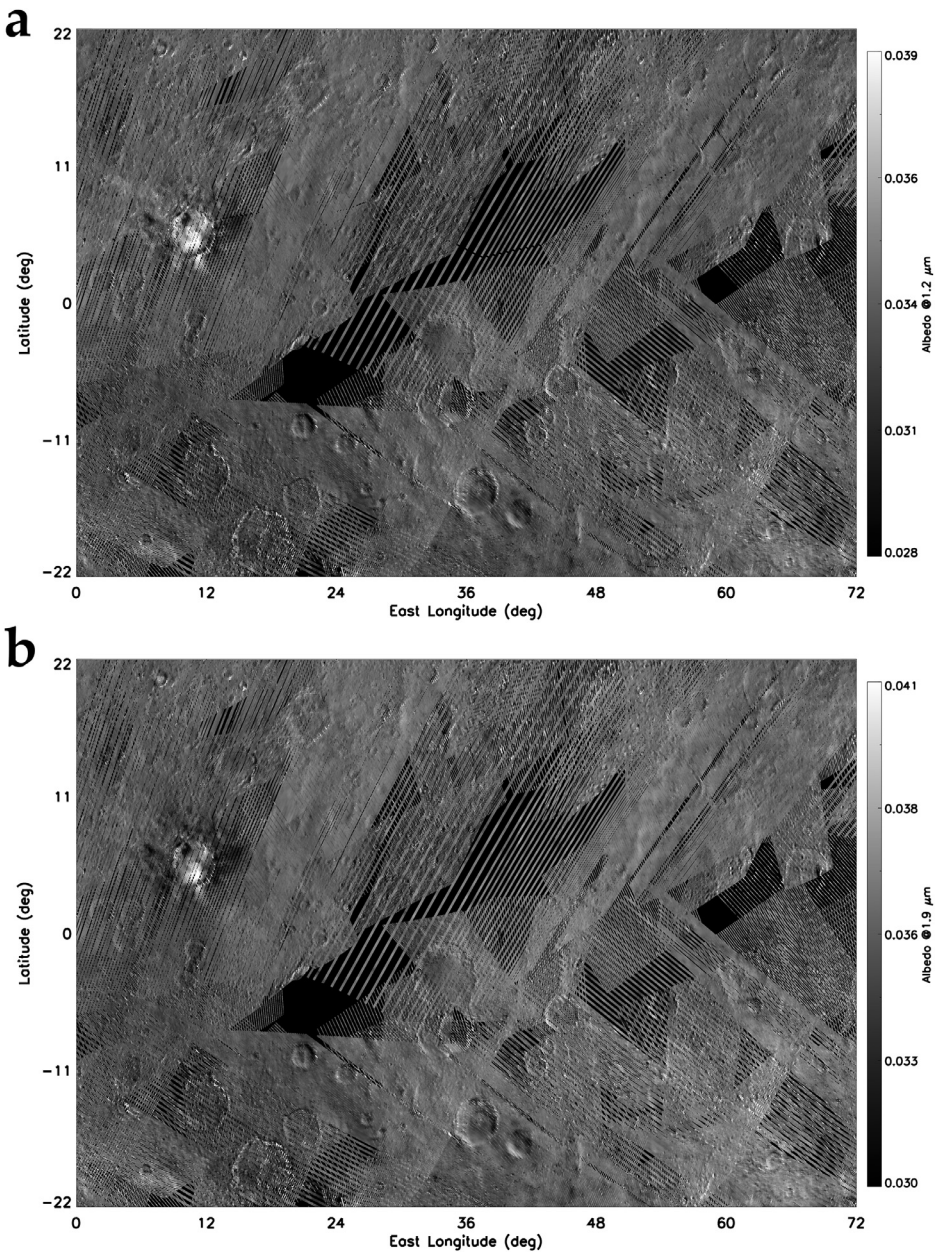

Fig. 3. a: Reflectance map of Ac-H-6 Haulani, obtained through photometric correction of VIR data acquired at 1.2 μm in the Survey and HAMO mission phases, interpolated on a grid with a fixed resolution of ~140 m/pixel, photometrically corrected by using the method described by Ciarniello et al. (2017), i.e. a Hapke photometric correction to standard observation geometry ($i = 30°$, $e = 0°$, $\alpha = 30°$). **b:** Reflectance map of Ac-H-6 Haulani, obtained through photometric correction of VIR data acquired at 1.9 μm in the Survey and HAMO mission phases, interpolated on a grid with a fixed resolution of 140 m/pixel. The same photometric correction of (**a**) was applied. In both maps, disconnected lines within a given image are due to the high instantaneous speed of the ground footprints (i.e., projections of the spectrometer's slit) in the HAMO phase.

quadrangle is ~9.5 km, with the deepest part (down to ~5.6 km below the reference ellopsoid) corresponding to a crater floor located at 22.0°N/17.3°E in the borderland between quadrangle Ac-H-6 Haulani and quandrangle Ac-H-2 'Coniraya', and to the floor of crater Kondos close to the southern edge, and the highest elevations (up to ~3.8 km above the reference ellipsoid) concentrated in the latitude range 15°S to 20°N and in the longitude range 20–60°E. The available datasets permit investigation of possible correlations between variations in reflectance, color and mineralogy, and the presence of hills and depressions. The topographic map also serves as a monitoring tool, allowing one to determine whether an observed variation in spectral indicators is reliable and not simply due to the combination of local topography and instantaneous solar illumination (see Section 3.1).

4.2. 1.2-μm and 1.9-μm reflectances

Reflectance maps obtained in the near infrared range at 1.2 μm and 1.9 μm, with the method briefly addressed in Section 3.1 (Fig. 3), are consistent with the reflectance map obtained by FC in the visual range and confirm that the floor and ejecta of crater Haulani are a patchwork of inherently bright and dark material units also at near-infrared wavelengths.

In particular, the highest reflectance values (~0.04 at both 1.2 μm and 1.9 μm) are recorded in the central and southern floor of the crater as well as in the ejecta that stretch to the south and the western inner wall, while relatively dark materials at these wavelengths (reflectance ~0.03) are found in the northern inner wall, in the ejecta that extend towards the east and southwest

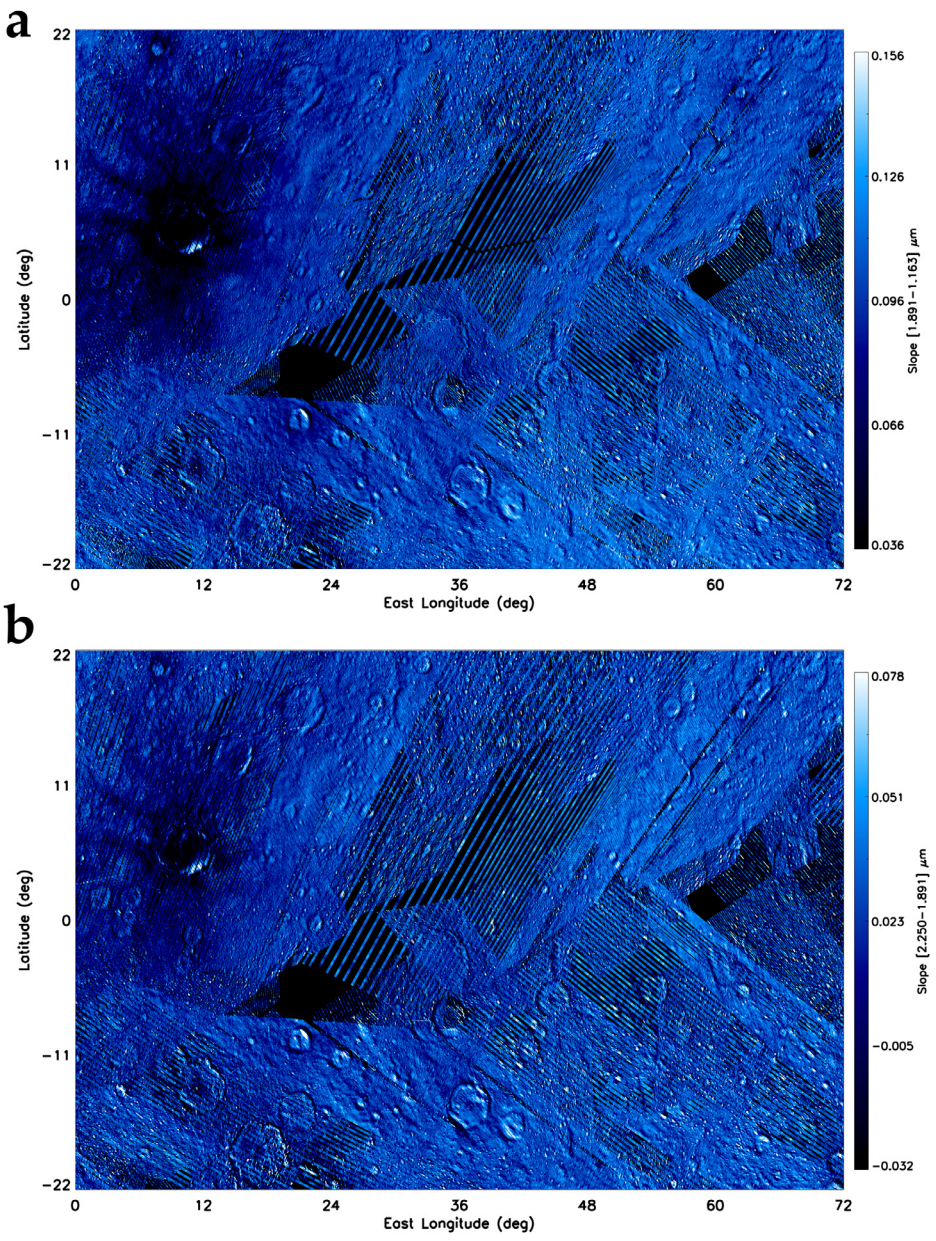

Fig. 4. Two spectral slopes, calculated in the near infrared range 1.163–1.891 μm (**a**) and 1.891–2.250 μm (**b**) on the basis of VIR infrared data. These spectral slopes are essentially consistent with the spectral slope obtained from FC data in the visual range 0.555–0.829 μm at higher spatial resolution (Fig. 2e): i.e., it is confirmed that crater Haulani generally corresponds to a neat reduction in spectral slopes, with negative values found in the middle of its floor, the western inner wall and the ejecta closer to the rim. In both maps, disconnected lines within a given image are due to the high instantaneous speed of the ground footprints (i.e., projections of the spectrometer's slit) in the HAMO phase. (For interpretation of the references to color in this figure legend, the reader is referred to the web version of this article.)

directions in the vicinity of the crater's rim, and in a distinct patch in the ejecta that extends to the west, a short distance from the rim. On the large asteroid Vesta, which was the previous target of the Dawn mission, impact craters often expose layers of both dark and bright material. In that case, the bright layers correspond to fresh pyroxenes processed by relatively little space weathering (McCord et al., 2012; Zambon et al., 2016). Conversely, bright spots on Ceres are thought to be the result of phenomena like cryovolcanism (Russell et al., 2016) and post-impact hydrothermal activity (Bowling et al., 2016).

The rest of the quadrangle shows a substantial uniformity in the infrared reflectance values, which is revealed by the narrow range of values in the gray colorbars.

4.3. Near-infrared spectral slopes

The two spectral slopes computed in the near infrared range: 1.163–1.891 μm and 1.891–2.250 μm (Fig. 4) are consistent with the spectral slope in the visual range 0.555–0.829 μm at higher spatial resolution (Fig. 2e): i.e., it is confirmed that crater Haulani generally corresponds to a substantial reduction in spectral slopes' values, with negative values found in the middle of its floor, the western inner wall and the ejecta closer to the rim, while mass wasting material found in the southeastern inner wall shows positive values of spectral slope similar to those measured in terrains found in the eastern side of the quadrangle (Stephan et al., 2017a). Other very small values of spectral slope, though not necessarily negative in the near infrared range, are found in the northeastern ejecta of

Please cite this article as: F. Tosi et al., Mineralogical analysis of the Ac-H-6 Haulani quadrangle of the dwarf planet Ceres, Icarus (2017), http://dx.doi.org/10.1016/j.icarus.2017.08.012

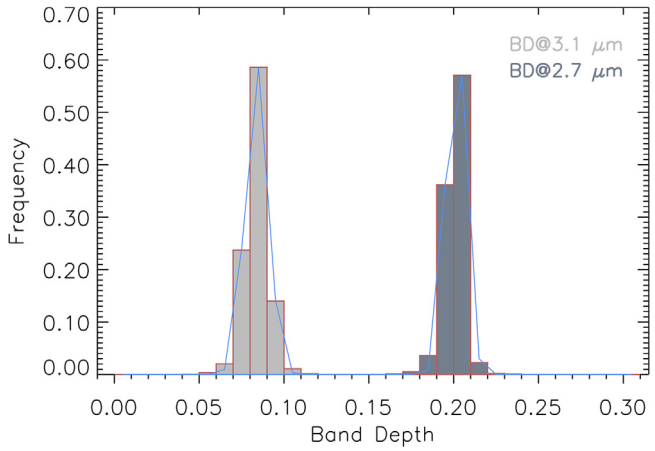

Fig. 5. Histograms of 2.7-μm band depth (BD27) and 3.1-μm band depth (BD31) values measured across quadrangle Ac-H-6 (after photometric correction), displayed in dark gray and light gray colors, respectively. A Gaussian fit is superimposed in the light blue color. The most recurrent values are in the range 0.16–0.24 (average value 0.201) for BD27 and 0.04–0.12 (average value 0.083) for BD31. (For interpretation of the references to color in this figure legend, the reader is referred to the web version of this article.)

a small unnamed crater located near the northern border of the Ac-H-6 quadrangle, centered at 20.7°N/7.6°E.

A different behavior in the spectral slopes between the visual range highlighted in the high-resolution FC mosaic (Fig. 2e) and VIR mosaics highlighted in Fig. 4 (i.e., local trends of spectral slopes in the visual range which seem to be neutral in the near infrared) is most likely indicative of the age of those materials, and therefore of space weathering processes.

The blue material becomes apparent in morphologically smooth areas, with flow features appearing morphologically smooth at the highest resolution images (35 m per pixel) obtained in the LAMO mission phase (Krohn et al., 2016; Stephan et al., 2017a). Physical alteration such as amorphization and aggregation of small-grained phyllosilicate-rich material and even heating up and melting the impacted surface material to moderate temperatures is expected in case of low-velocity impact events, which could explain the observed blue spectral slope (Stephan et al., 2017a). As small scale roughness is thought to dominate the scattering behavior (Shepard and Helfenstein, 2007), the bright, blue ejecta of craters that show evidence for flows, like Haulani, may in fact be physically smooth. High albedo, blue color, and physical smoothness all appear to be indicators of youth (Schröder et al., 2017).

4.4. 2.7-μm and 3.1-μm band depths

Fig. 5 shows histograms related to the frequency of the band depths at 2.7 μm and 3.1 μm (hereafter BD27 and BD31) values measured across the Haulani quadrangle, sampled with a 0.01 bin width.

Consistent with the average reflectance spectrum of the surface of Ceres as measured by VIR, where the absorption centered at 2.72–2.73 μm is broader than the absorption centered at 3.05–3.1 μm (see Fig. 1), BD27 is greater than BD31, with most recurrent values in the range 0.16–0.24 (average value 0.201) for BD27 and 0.04–0.12 (average value 0.083) for BD31. These two distributions have a narrow width, with extremely similar maximum values of frequency and comparable shapes hardly modeled by a Gaussian fit. This evidence demostrates the goodness of photometric correction, and testifies a homogeneous distribution of the abundance of the featureless spectral endmember across the entire quadrangle. For comparison, in other nearby quadrangles of Ceres the observed statistics may show a slightly different distribution (e.g., Zambon et al., 2017b, this issue).

This aspect is also important to associate the values of BD27 and BD31 that we observe to relative abundances of Mg-rich and NH_4-rich phyllosilicates, respectively. As anticipated in Section 3.1, the band depth value, which is indicative of a mineral's abundance, may also be affected by the presence of opaque phases and by the grain size. In order to quantify abundance values, a spectral unmixing model has to be applied to the observed spectral data, which is beyond the scope of this work, while it is addressed elsewhere for a narrower region within quadrangle Ac-H-6, covering only crater Haulani (Tosi et al., 2017, under review). However, from the spectral unmixing modeling carried out previously to establish the global average mineralogy of Ceres, it turns out that best fits with respect to the average reflectance spectrum of Ceres as measured by VIR are obtained by using antigorite with a grain size of 90 μm, Mg-carbonates with a grain size of 10 μm, and a featureless dark component with a grain size of 80 μm (the grain size for NH_4-rich phyllosilicates could not be determined unequivocally) (Fig. 4a and Extended Data Table 2 in De Sanctis et al., 2015). So, under the reasonable assumption that these grain size values are recurrent on a broadly regional scale including quadrangle Ac-H-6, our BD27 and BD31 values may be associated to mineral abundances rather than to variations in the grain size distribution.

Fig. 6 reveals a map of the BD27 and BD31 values across the Haulani quadrangle. First, a comparison with the topographic map shown in Fig. 2f shows that the band depth in most cases does not follow the trend of the topography, suggesting that our photometric correction properly removes the effects of topographic slope (see Section 3.1). The most striking result is that low BD27 and BD31 values are associated with crater Haulani's floor and ejecta (most notably those extending in the north–south direction), which appear bluish in FC-derived maps in both the Clementine and enhanced presentations, except in the southeastern inner wall of the crater. This evidence indicates an overall net decrease in the abundance of Mg- and NH_4-bearing phyllosilicates in the region of crater Haulani, compared to the surrounding terrains and geologic units. Other smaller patches showing a similar decrease in these two BD values are located in the floors of the craters Shakaema, Anura and Kondos. In particular, in the case of Kondos a decrease of the BD31 value is observed west of the crater, not followed by a proportional decrease in the BD27 value. Conversely, the southeastern region of the quadrangle, corresponding to the cratered (oldest) terrain unit, is characterized by higher values of BD27 and BD31. Fig. 7 shows a direct comparison between the reflectance spectra of these regions and the average reflectance spectrum of quadrangle Ac-H-6 as a whole.

High values of BD27 not matched by equally high values of BD31 are found in a small unnamed crater centered at about 9.9°S/40.9°E, while the unnamed crater centered at 20.7°N/7.6°E shows an opposite behavior, with its northern ejecta depleted in Mg-bearing phyllosilicates, but its floor showing an enhancement in NH_4-bearing phyllosilicates compared to surrounding terrains.

In summary, in quadrangle Ac-H-6 there is a general trend in values BD27 and BD31, and therefore in the abundances of Mg-rich and NH_4-rich phyllosilicates, to increase by moving from the northwest to the southeast. However, this trend is strongly influenced by crater Haulani, and to a lesser extent by other larger craters such as Kondos, Anura and Shakaema as well as smaller unnamed craters. Their formation significantly altered an otherwise smooth transition in the abundances of these two mineral species across this region.

4.5. BD27 versus BD31

We next evaluate the possible correlation between the BD27 and BD31 values. In this case, a high degree of correlation is indicative of a strong (intimate) mixture between the OH-bearing and

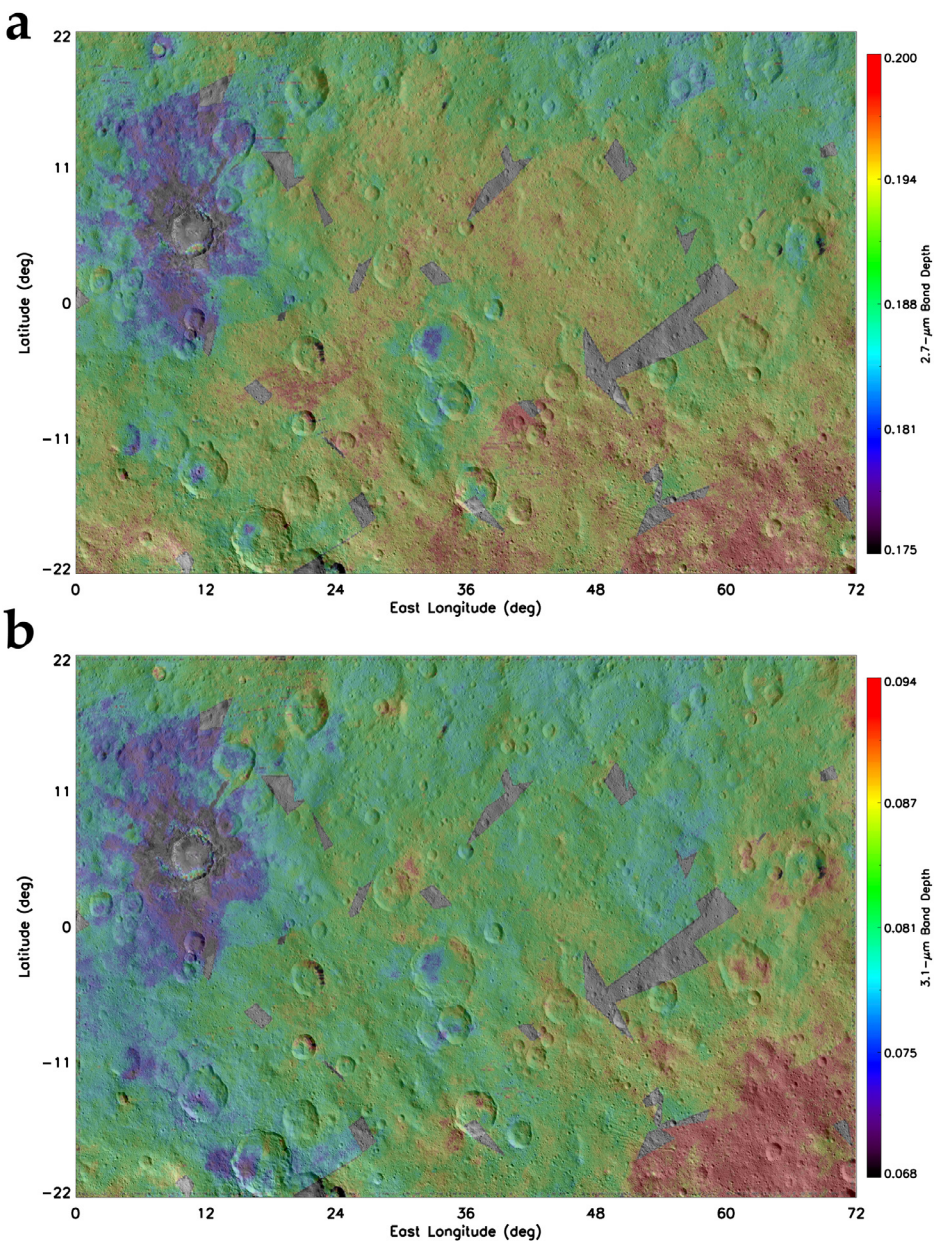

Fig. 6. Distribution of 2.7-μm band depth (BD27) (**a**) and 3.1-μm band depth (BD31) (**b**) values across the Haulani quadrangle, derived from VIR data. These band depths are sensitive to the abundance of magnesium-bearing phyllosilicates and ammoniated phyllosilicates, respectively, and to the presence of opaque contaminants. The overall distribution spans from lower depth (dark blue to blue) to greater depth (red to dark red). The floor and ejecta associated with the spectrally distinct material of crater Haulani have shallower BD27 and BD31 values. The Haulani crater itself displays spectral variations in its interior: BD values are shallower on the floor and stronger in the southeastern and northern walls. Small values are also found elsewhere throughout the quadrangle: other smaller patches showing a similar (but not necessarily parallel) decrease in these two BD values are located in the floors of the craters Shakaema, Anura and Kondos. (For interpretation of the references to color in this figure legend, the reader is referred to the web version of this article.)

NH_4-bearing phyllosilicates, while moderate-to-low correlation values hint to areal mixtures. Fig. 8a is a density scatterplot of BD27 as a function BD31. Because there is one big cluster of points, with most data concentrating close to the most recurrent values (0.201 for BD27 and 0.083 for BD31, respectively), a linear model proves inadequate to describe the trend of the ratio of Mg-rich/NH_4-rich phyllosilicates: as revealed by the chi-square, the distribution is essentially non-linear, and the average coefficient of determination is moderate-to-low, meaning that a substantial correlation between these two variables is not found anywhere throughout the quadrangle, but only for specific geologic features found at the local scale.

By mapping the value of the ratio between the measured BD27 and the BD27/BD31 linear approximation (Fig. 8b), one can see that points with BD27 values significantly lower than the linear model displayed in Fig. 8a, i.e. with a lower value of the ratio Mg-rich/NH_4-rich phyllosilicates, generally correspond to the area of crater Haulani (floor, rim and ejecta, especially those extending in the north and south directions) and the northeastern corner of the quadrangle. This indicates that the Mg- depletion extends further from Haulani than the NH_4-depletion. Conversely, values significantly higher than the linear model, i.e. with a higher value of the ratio Mg-rich/NH_4-rich phyllosilicates, concentrate in the southern and southwestern part of the quadrangle, particularly in Wangala Tholus (notable exceptions being the floors of craters Shakaema, Anura, Kondos and Piuku), and in the middle-northern quadrant.

Fig. 9 is divided in two panels. Fig. 9a represents a 2D scatterplot of BD31 vs. BD27 for the entire surface of Ceres. Fig. 9b shows

Please cite this article as: F. Tosi et al., Mineralogical analysis of the Ac-H-6 Haulani quadrangle of the dwarf planet Ceres, Icarus (2017), http://dx.doi.org/10.1016/j.icarus.2017.08.012

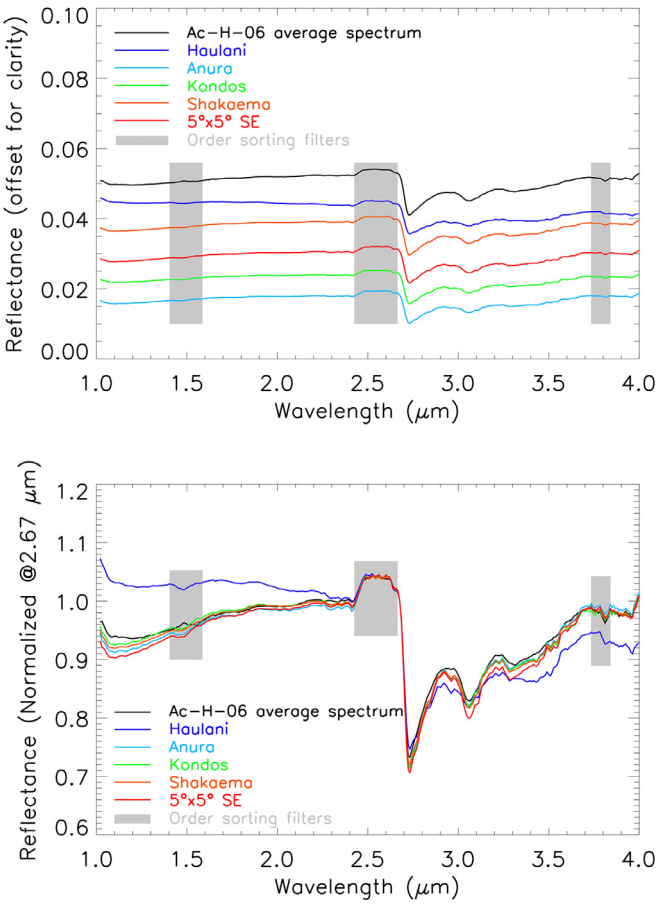

Fig. 7. a: Reflectance spectra of craters Haulani (blue), Anura (cyan), Kondos (green), Shakaema (orange), and of a 5° by 5° region (Latitude 17–22°S, Longitude 60°E-65°E) in the southeastern region of quadrangle Ac-H-6, as observed by VIR in the HAMO mission phase (pixel resolution ~0.38 km), compared to the average reflectance spectrum of the entire quadrangle (black). An arbitrary offset is applied for clarity. Gray boxes highlight the spectral counterparts (position and width) of three order sorting filters placed on top of the VIR infrared focal plane, which induce systematic artifacts in VIR data. **b:** Same spectra of panel (**a**), normalized at 2.67 μm, a wavelength which is unaffected by both known spectral features and instrumental artifacts. Haulani stands out to have a blue spectral slope and shallower band depths at 2.7 and 3.1 μm compared to other larger and older craters and to cratered terrain in the southeast. (For interpretation of the references to color in this figure legend, the reader is referred to the web version of this article.)

the same 2D scatterplot of Fig. 9a superimposed on a four-color palette, where the color code is designed specifically to take advantage of the band depth information simultaneously: here colors are such that blue indicates that the two absorption bands are both strong, orange means that the two absorption bands are both weak, green indicates a strong 2.7-μm absorption band and a weak 3.1-μm absorption band, and magenta indicates a strong 3.1-μm absorption band and a weak 2.7-μm absorption band. This is motivated by combining two maps in one, without the color ambiguity that result from classical three color composites (RGB).

Fig. 9 provides a convenient way to map these abundances simultaneously on the surface of quadrangle Ac-H-6. In this regard, Fig. 10 displays two color maps. The first map (Fig. 10a) uses a four-color, two-dimensional table, where all VIR pixels on the map are represented by a color (not black). This is very similar to representing one parameter with a one-dimension color scheme (a ramp), where the parameter values are represented between a minimum and a maximum, and are scaled to the number of color levels. In the second map (Fig. 10b), only the purest compositions are represented by colored pixels, while all the others are dark. This is justified by assuming that the surface composition with the highest population likely results from mixtures, and therefore it does not represent pure chemistry or mineralogy. Pure compositions are useful to identify the origins of surface materials and interpret the processes involved in their formation.

The two maps in Fig. 10 overall confirm a substantial depletion in both Mg-rich and NH_4-rich phyllosilicates in the floor and ejecta of crater Haulani (except in its southeastern and northern inner walls), while the rest of the quadrangle shows a mineralogy similar to the global average mineralogy of Ceres. Indeed, variability in the relative abundances of these two main mineral phases can also be found locally, i.e. in the floors and ejecta of other craters as discussed before, but to a much lesser extent compared to crater Haulani.

4.6. 4.0-μm band center and band depth

While global maps of carbonates, detected on the basis of VIR data on Ceres, are addressed elsewhere (Carrozzo et al., 2017a, this issue), a significant result obtained for the Ac-H-6 quadrangle (Fig. 11) is that the signature of carbonates is usually centered at 3.95 μm, i.e. indicative of Mg- or (Mg,Ca)-rich carbonates like in most of Ceres' surface, except in specific areas found at the local scale.

In crater Haulani's western and northwestern inner walls, in the eastern inner wall and in some ejecta that propagate towards the west and northwest, the band center moves to 3.97 μm, which is diagnostic of Ca-carbonates or alternatively a mixture of (Mg,Na)-rich carbonate endmembers in the mineralogy of those areas (Palomba et al., 2017b, this issue). In the southern rim and the ejecta departing from here to the south, the band center may move up to 3.99 μm, which is possibly diagnostic of Na-carbonates in very specific sites.

This evidence is not observed in the rest of the quadrangle, except for a distinct patch in the floor of the 44-km crater Kondos, located close to the southern edge of Ac-H-6, and in the ejcta of a small, fresh unnamed crater located at 20.7°N/7.6°E, which instead is located close to the northern edge of Ac-H-6. Both these sites reveal a local enhancement in the abundance of Ca-rich carbonates compared to surrounding terrains.

4.7. Surface temperature

In the case of the Haulani quadrangle, we have separately considered surface temperature data retrieved from VIR infrared observations obtained only in the Survey phase, in order to maintain uniformity in both the spatial resolution and the local solar time or LST (the majority of the observations acquired in this mission phase took place in the cerean morning between 10 h and 12 h LST). For this reason, there are major gaps in coverage, as revealed by Fig. 12. The surface temperature map is accompanied by a map of the solar incidence angle, so as to enable a direct comparison with the instantaneous solar illumination.

VIR-derived temperature images reveal that the only substantial thermal signature detectable in the Ac-H-6 quadrangle corresponds to crater Haulani's mountainous region in the middle of its floor, which is ~8 K cooler than surrounding terrains observed at the same local solar time and under similar solar illumination, and – to a lesser extent – part of its bright rim and ejecta, hinting that the albedo of fresh material excavated by the impact, together with a higher compactness of this material in the crater's peak, may be responsible for the observed behavior. Conversely, thermal shades in the rest of the quadrangle, at least to the spatial scale investigated by VIR in this dataset, can be generally explained by solar illumination combined with the local topography at the time of the observation, which suggests that the thickness of the regolith in this region, regardless of albedo differences (that are anyway only

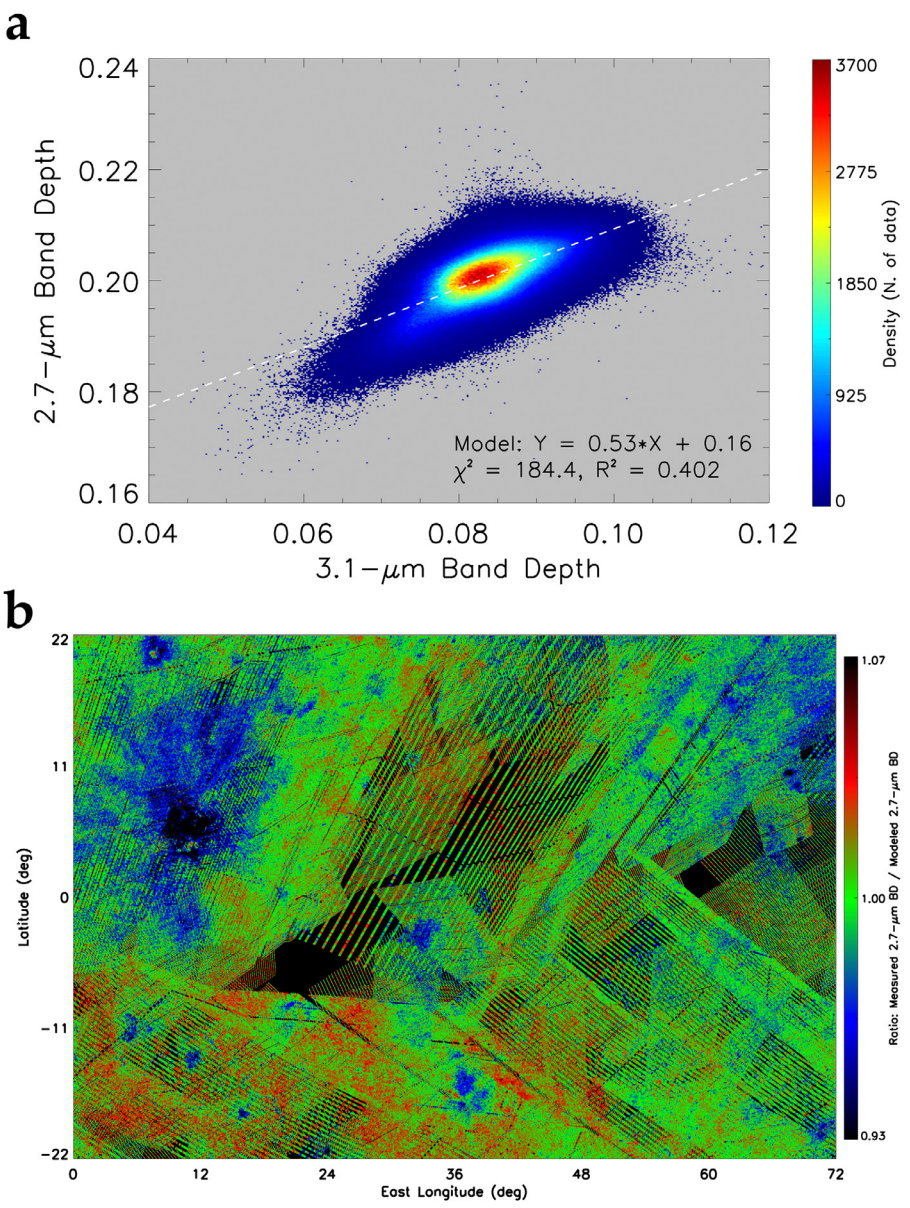

Fig. 8. a: Density scatterplot of 2.7-μm band depth (BD27) as a function of 3.1-μm band depth (BD31) computed for the quadrangle Ac-H-6. A linear fit model (white dashed line) is superimposed on the distribution (values of the chi-square (χ^2) and the coefficient of determination (i.e., the squared correlation coefficient R^2) are also provided). Most data concentrate around the average values. The cluster shows a large spread and a moderate-to-low correlation in the linear fit model. **b:** Ratio between the measured 2.7-μm band depth and the BD27/BD31 linear fit model. This map shows where the surface material departs from an ideally linear correlation between the abundance of the two major mineral species. Dark blue to blue colors mark locations that have shallower BD27 than the linear model, while red to dark red shades mark locations that have larger BD27 than the linear model. If BD27 was perfectly correlated with BD31, this map would appear uniformly green. In the map, disconnected lines within a given image are due to the high instantaneous speed of the ground footprints (i.e., projections of the spectrometer's slit) in the HAMO phase. (For interpretation of the references to color in this figure legend, the reader is referred to the web version of this article.)

relevant for crater Haulani) is generally large enough to mask any inhomogeneity in terms of density (e.g., outcrops of compact material, pebbles or very coarse grain size) and/or in the thermal conductivity (Tosi et al., 2014).

Crater Haulani's thermal signature was first noticed in VIR data acquired in February 2015 during the Approach phase, which covered a substantial fraction of the dayside of Ceres under a solar phase angle of 44.5° At coarse spatial resolution (11.4 km/px), the region of crater Haulani already showed a distinct thermal contrast, being ~5 K cooler than the rest of the surface as observed at 11 h LST (Tosi et al., 2015a). The spatial scale of those data could safely rule out shading effects due to local topography. Ceres is expected to have a low thermal inertia, albeit greater than Vesta's thermal inertia at global and broadly regional scale (Titus, 2015; Hayne and Aharonson, 2015). The maximum diurnal temperature is a stronger constraint than other temperature points sampled on the dayside, since this maximum shifts from local noon to the afternoon as the thermal inertia of the explored area increases. Therefore, the slower response to instantaneous solar illumination, measured by VIR in the late cerean morning, could be indicative of a substantial departure (i.e., increase) in thermal inertia compared to the global average, which is consistent with the higher compactness of Haulani crater's central mound and, to a lesser extent, of its surrounding features.

5. Discussion and conclusions

Ac-H-6 'Haulani' is one of the most interesting quandrangles in the Ceres equatorial belt, and on this dwarf planet in general. In this work we have undertaken a thorough investigation of

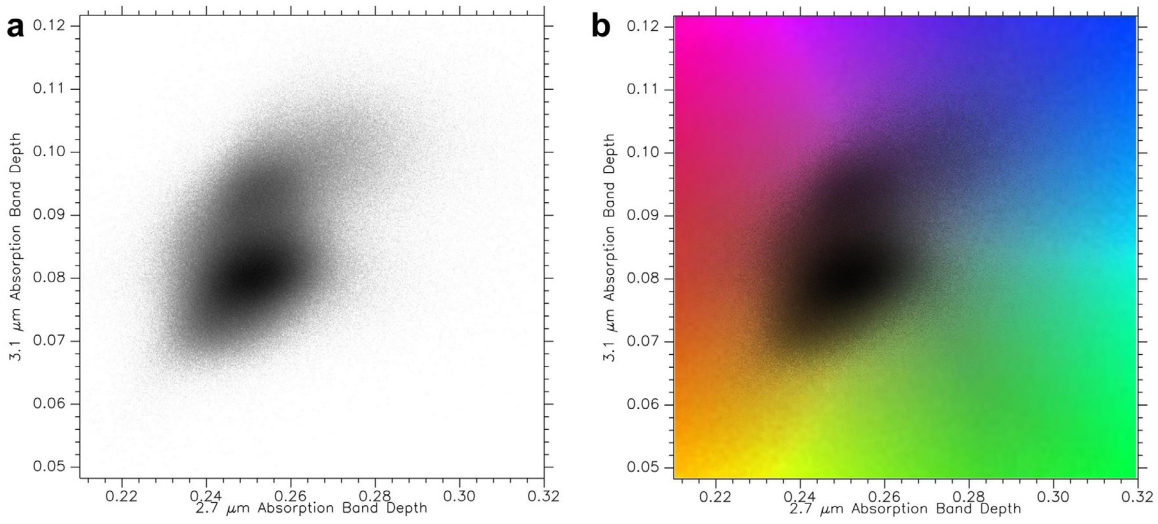

Fig. 9. a: 2D scatterplot of 2.7-μm band depth (BD27) as a function of 3.1-μm band depth (BD31) computed for the entire surface of Ceres. **b:** Same 2D scatterplot of (**a**) superimposed on a four-color scheme that also provides a legend for Fig. 10. Materials depleted in both Mg-rich phyllosilicates and NH_4-rich phyllosilicates appear in yellow–orange colors, while materials enriched in both Mg-rich phyllosilicates and NH_4-rich phyllosilicates are displayed in blue. The green color marks materials with enhanced abundance of Mg-rich phyllosilicates and depletion of NH_4-rich phyllosilicates, while the purple color highlights an opposite situation, i.e. materials depleted in Mg-rich phyllosilicates and a relatively high abundance of NH_4-rich phyllosilicates. (For interpretation of the references to color in this figure legend, the reader is referred to the web version of this article.)

the mineralogy of the Haulani quadrangle as a whole, using various techniques designed to complement and expand the analysis performed in previous work, providing quantitative results that can be directly compared with those obtained for other cerean quadrangles, which are discussed in other papers of this special issue by means of similar techniques (Carrozzo et al., 2017b, this issue; Combe et al., 2017b, this issue; De Sanctis et al., 2017b; Longobardo et al., 2017, this issue; Palomba et al., 2017a; Raponi et al., 2017, this issue; Singh et al., 2017, this issue; Stephan et al., 2017b, this issue; Zambon et al., 2017b, this issue).

The two widespread mineral species discussed in this article, i.e. magnesium-bearing phyllosilicates and ammoniated phyllosilicates, respectively identified by diagnostic spectral signatures centered at ~2.7 and ~3.1 μm, show a general enrichment in Mg-rich phyllosilicates from northwest to southeast, which corresponds to the oldest geologic unit (cratered terrain). The distribution of the featureless spectral endmember, which may affect the band depths, is also overall uniform, and no obvious correlation between mineralogy and topography combined with the instantaneous solar illumination is observed in most of the Haulani quadrangle.

In a broader context, these findings are overall consistent with the general mineralogy observed in nearby quadrangles of Ceres. In quadrangle Ac-H-10 'Rongo', located west of quadrangle Haulani, Mg-bearing phyllosilicates are depleted in the easternmost region including crater Rongo, and a broader area of depletion is observed in the southwestern quadrant, while the distribution of NH_4-bearing phyllosilicates is relatively uniform, except in the easternmost region, which also shows a net depletion (Zambon et al., 2017b, this issue). Such depletion in both these two main mineral species is consistent with what we observe in Ac-H-6 west of crater Haulani, and represents a smooth transition between these two adjacent quadrangles. In quadrangle Ac-H-11 'Sintana', located south of quadrangle Haulani, the mineralogy is consistent with what we observe in the southeastern side of Ac-H-6, with magnesium-bearing phyllosilicates and ammoniated-phyllosilicates' band intensity that keeps increasing by going from low southern latitudes to the southernmost regions (De Sanctis et al., 2017b, this issue). Quadrangle Ac-H-2 'Coniraya', located north of quadrangle Haulani, includes several features of interest, such as the water ice-rich crater Oxo (Combe et al., 2016), the organics-rich crater Ernutet (De Sanctis et al., 2017a), and the pitted terrains-rich crater Ikapati (Sizemore et al., 2017). Here an overall increase in the band depth of magnesium-bearing phyllosilicates is observed from east to west, particularly in the soutwestern corner of the quadrangle, not necessarily correlated with an equal decrease in the band depth diagnostic of ammoniated phyllosilicates (Raponi et al., 2017, this issue). Finally, quadrangle Ac-H-7 'Kerwan', located east of quadrangle Haulani, overall shows enrichment in Mg-phyllosilicates in the southern region compared to the northern region, and depletion of NH_4-rich phyllosilicates in the northwestern region. Again, the spectral indices of these two major mineral species do not display a substantial correlation across most of the quadrangle, except in specific regions of interest observed at the local scale (Palomba et al., 2017a, this issue).

From a mineralogical standpoint, the most prominent surface feature in quadrangle Ac-H-6 is by far the 34-km crater Haulani, one of the youngest geologic features on Ceres, which in turn is made up by a complex system of geologic sub-units with different morphology and albedo (Krohn et al., 2017). The floor and the ejecta of crater Haulani display one of the most negative ('bluest') spectral slopes at visible to near infrared wavelengths across the entire surface of Ceres. This blue slope is generally associated with bright material units, which is indicative of a younger age and therefore less processed material. The bright and bluest materials observed in and around crater Haulani correspond to a substantial decrease in both the band depths of spectral features diagnostic of Mg-rich and NH_4-rich phyllosilicates. In the ejecta, this depletion is more prominent in the north–south direction and at relatively short ranges from the crater, with the depletion of Mg-rich phyllosilicates that extends farther away. The correlation observed between these two spectral indices in Haulani's ejecta is increasingly weaker in moving away from the crater. One physical justification might be that the energy required to release the hydroxide ion OH^- from a phyllosilicate is less than the energy required to release the ammonium ion NH_4^+, due to the different strengths of these chemical bonds. The bluish ejecta of Haulani also extend westward, crossing the neighboring quadrangle Ac-H-10 Rongo. In that case, Haulani's ejecta still show depletion in both Mg-rich and NH_4-rich phyllosilicates, even though the two band depth values show a very

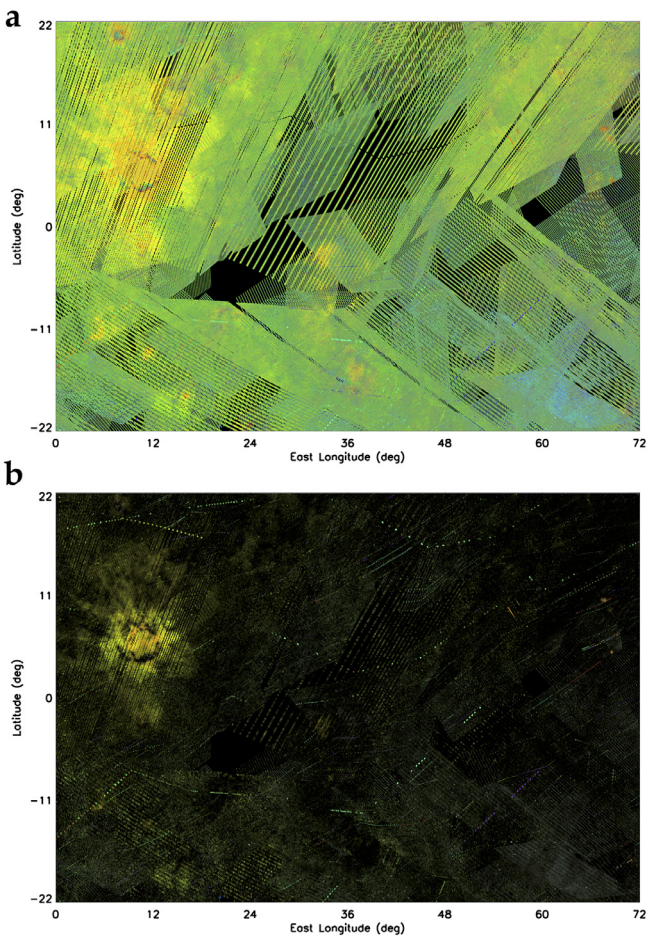

Fig. 10. a: Four-color representation of the two spectral parameters: 2.7-μm band depth (BD27) and 3.1-μm band depth (BD31). In this map, all VIR pixels are represented by a color according to the scheme defined in Fig. 9b: pairs of values (BD27, BD31) are scaled to (X, Y) coordinates of the color scheme. **b:** Same kind of map as (**a**), but in this case only the purest compositions are represented by colored pixels, while all the others are dark. This is obtained by masking the pixels that host the most frequent values in the pair of parameters. In both maps, disconnected lines within a given image are due to the high instantaneous speed of the ground footprints (i.e., projections of the spectrometer's slit) in the HAMO phase.(For interpretation of the references to color in this figure legend, the reader is referred to the web version of this article.)

weak correlation at large distance from the crater (Zambon et al., 2017b, this issue), consistent with our findings within quadrangle Ac-H-6.

While neither water ice nor peculiar hydrated minerals are observed today in the region of crater Haulani, considerable variability is recorded in its interior. Notable examples are mass wasting material found in the southeastern inner wall and some mass wasting patches located in the northern inner wall close to the rim, which show a positive spectral slope and an abundance of the main mineral species comparable to the average values recorded far from the crater.

Elsewhere in Ac-H-6, negative spectral slopes in the visible to near infrared range up to 2.25 μm are recorded in specific geologic features observed at the local scale, albeit with smaller absolute values compared to crater Haulani. Notable examples are the small crater at 13.7°S/11.2°E, in the middle of crater Anura's floor, and the ejecta of two unnamed small craters respectively located at 20.7°N/7.6°E and 10.0°S/21.0°E. Other local-scale features display negative spectral slopes in the visual range but not necessarily in the near infrared range up to 2.25 μm. Similarly, a decrease in the abundances of Mg-rich and NH_4-rich phyllosilicates is found also in other impact craters of varying size (including greater than Haulani's size). However, these occurrences do not affect large areas, but rather part of their floors and ejecta.

By examining the relationship existing between the values of the band depths at 2.7 and 3.1 μm in quadrangle Ac-H-6, no particular trend is highlighted, but a much stronger correlation is observed and mapped over those areas of crater Haulani that are substantially depleted in both the two major mineral species, compared to other features discussed in this paper where a similar depletion is observed.

Since mineralogy on Ceres at global and broadly regional scales is dominated by magnesium- and ammonium-bearing phyllosilicates, carbonates, and a spectrally featureless dark component (De Sanctis et al., 2015; Ammannito et al., 2016; Carrozzo et al., 2017a, this issue), one possible explanation is that the impact that created Haulani could have affected a portion of Ceres originally rich in hydrated and ammoniated material, penetrating the crust enough to excavate brighter and less processed material and causing intimate mixing between these mineral phases. This is consistent with the evidence that part of crater Haulani's floor is pitted terrain, which on Ceres likely form via the rapid volatilization of molecular H_2O (possibly water ice) entrained in shallow subsurface materials (Sizemore et al., 2017).

The work of Schmedemann et al. (2016) and Krohn et al. (2016) determined that the blue-sloped material is the youngest material on Ceres's surface and interpreted the association of flow features with impact craters as indication for highly fluidized material/impact melt (Stephan et al., 2017a). Because the shallow subsurface of Ceres may harbor water ice (Prettyman et al., 2017; Schmidt et al., 2017), the ejecta of a fresh crater like Haulani might have been initially a liquid water/phyllosilicate mixture, perhaps as a consequence of impact melting of subsurface water ice, that turned blue after desiccation (Schröder et al., 2017). The physical smoothness of the regolith is consistent with the initial fluid condition. Alternatively, spectral bluing would be caused by ultrafine (~50–100 nm in size) grains that strongly stick together forming larger agglomerates (tens of micrometer in size) and/or by a higher abundance of amorphous material (Stephan et al., 2017a). In both of these scenarios, space weathering, in terms of diurnal temperature variations and micrometeoritic impacts forming a regolith layer of fine-grained phyllosilicate dust, may be responsible for the fading of the blue color over time (Stephan et al., 2017a).

While nowadays the diagnostic absorptions of magnesium-bearing phyllosilicates and ammoniated phyllosilicates are much shallower in the floor of the crater, the impact properties have been able to preserve to some extent the original mineralogy in other specific areas, such as parts of the inner walls. On the other hand, Ca- and possibly Na-rich carbonates found in part of the walls, rim, floor and ejecta of crater Haulani, which are discussed separately both in a broader context (Carrozzo et al., 2017a, this issue; Palomba et al., 2017b, this issue) and specifically for crater Haluani itself (Tosi et al., 2017, under review), are also very likely a byproduct of the impact event and are related to brighter material units, similar to what has been observed in other specific places on Ceres, most notably in crater Occator (De Sanctis et al., 2016). An enrichment in carbonates, especially when associated with a lower local content in OH-rich and NH_4-rich phyllosilicates, is one evidence in support of intense hydrothermal processes triggered by impact events, similar to those observed in other specific sites on Ceres (De Sanctis et al., 2016; Combe et al., 2017a, this issue). In this regard, it is worth noting that elsewhere in quadrangle Ac-H-6 other impact craters larger than Haulani do not show the same contrast in terms of mineralogical indices (albedo, reduced or even negative spectral slopes, depletion in Mg-rich and NH_4-rich phyllosilicates, presence of Ca- and Na-carbonates), in support of the hypothesis that initial conditions of in terms of shallow subsurface

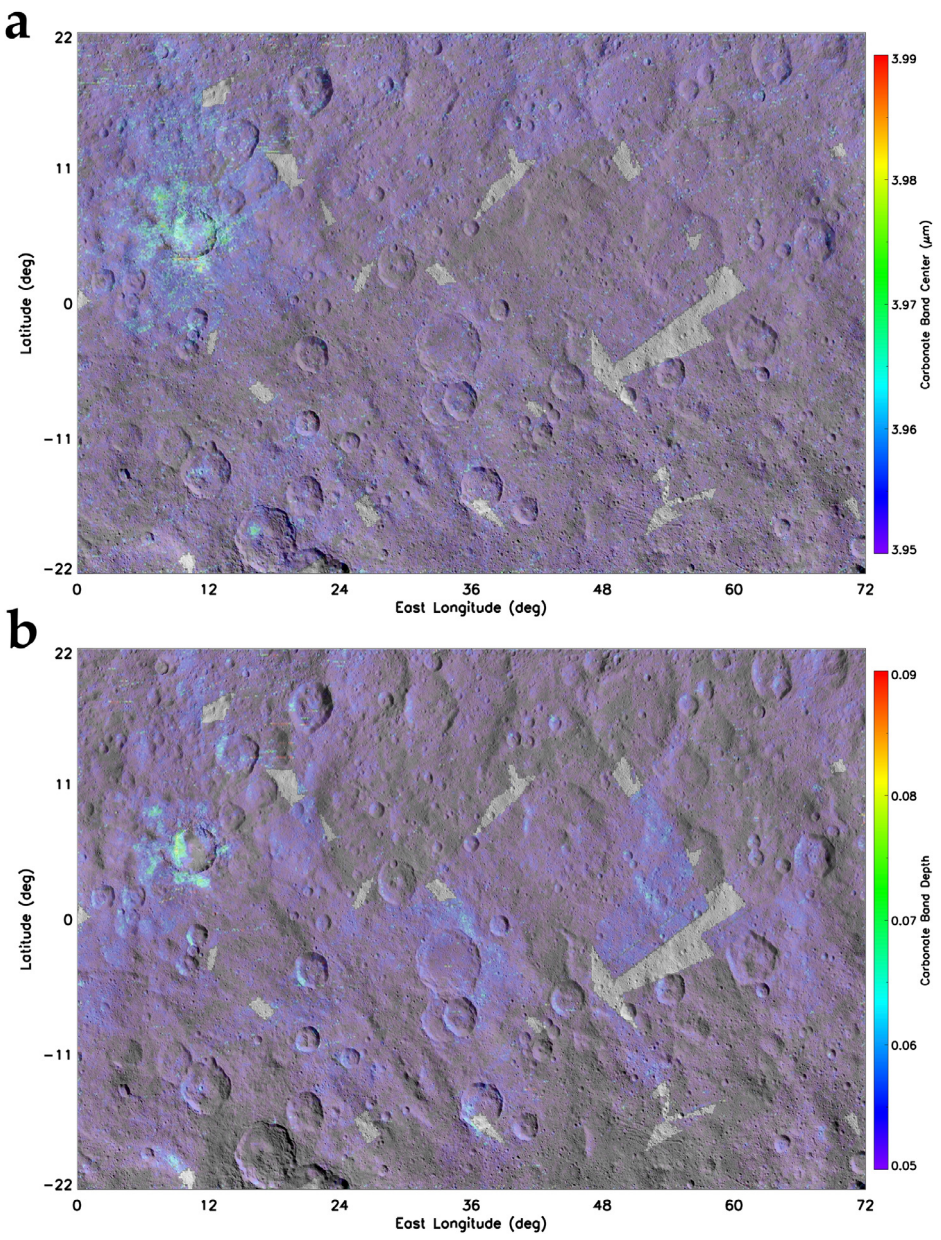

Fig. 11. Distribution of 4.0-μm band's center (**a**) and band depth (**b**) values across quadrangle Ac-H-6 Haulani, derived from VIR data. These parameters are respectively sensitive to the composition and abundance of carbonate minerals. The overall distribution spans from Mg- or (Mg,Ca)-rich carbonates (violet to blue) to Na-rich carbonates (red) (**a**), and from lower depth (violet to blue) to greater depth (red) (**b**). Local enhancement of Ca-rich and possibly Na-rich carbonates is found locally in the region of crater Haulani, most notably in its western inner wall and ejecta closest to the southern rim. Other evidences of Ca-rich carbonates are found in part of Kondos crater's floor and in the ejecta of a fresh unnamed crater located at 20.7°N/7.6°E, even though with smaller concentrations compared to crater Haulani. (For interpretation of the references to color in this figure legend, the reader is referred to the web version of this article.)

composition and the characteristics of the impact event (e.g., specific energy) may prove crucial in triggering these processes, which would otherwise be widespread on the surface. Within quadrangle Ac-H-6, only the 44-km crater Kondos, which dug deeper into the crust, shows some mineralogical similarity with respect to crater Haulani, even though this evidence is found in a much smaller area, namely part of its floor. This suggests that craters older than Haulani have experienced relaxation and mass wasting phenomena that somehow mixed pre- and post-impact composition, ultimately reducing the extension and contrast of the carbonate-rich areas and achieving, over time, an intermediate abundance of magnesium-rich phyllosilicates and ammoniated phyllosilicates.

Crater Haulani shows a distinct thermal signature, being cooler than the surrounding regions observed by VIR under similar illumination conditions and during maximum diurnal insolation, which suggests a higher thermal inertia, i.e. a local slower response to instantaneous insolation compared to the average surface of Ceres. This thermal contrast does not arise in the pitted part of the floor (Sizemore et al., 2017), but rather in the central mound and in the ejecta closer to the rim, matching bright material with the bluest spectral slope. In this regard, bluish material observed in other surface features on Ceres does not display an equally prominent thermal contrast. One explanation bounding mineralogical and thermal evidences is that part of the material that melted during the impact event may have remained relatively compact up to now, which would explain the higher thermal inertia observed in those specific sites.

Although the variety of colors and spectral information that the Dawn mission was able to get in the Haulani quadrangle is somewhat peculiar compared to many other places on Ceres, the picture

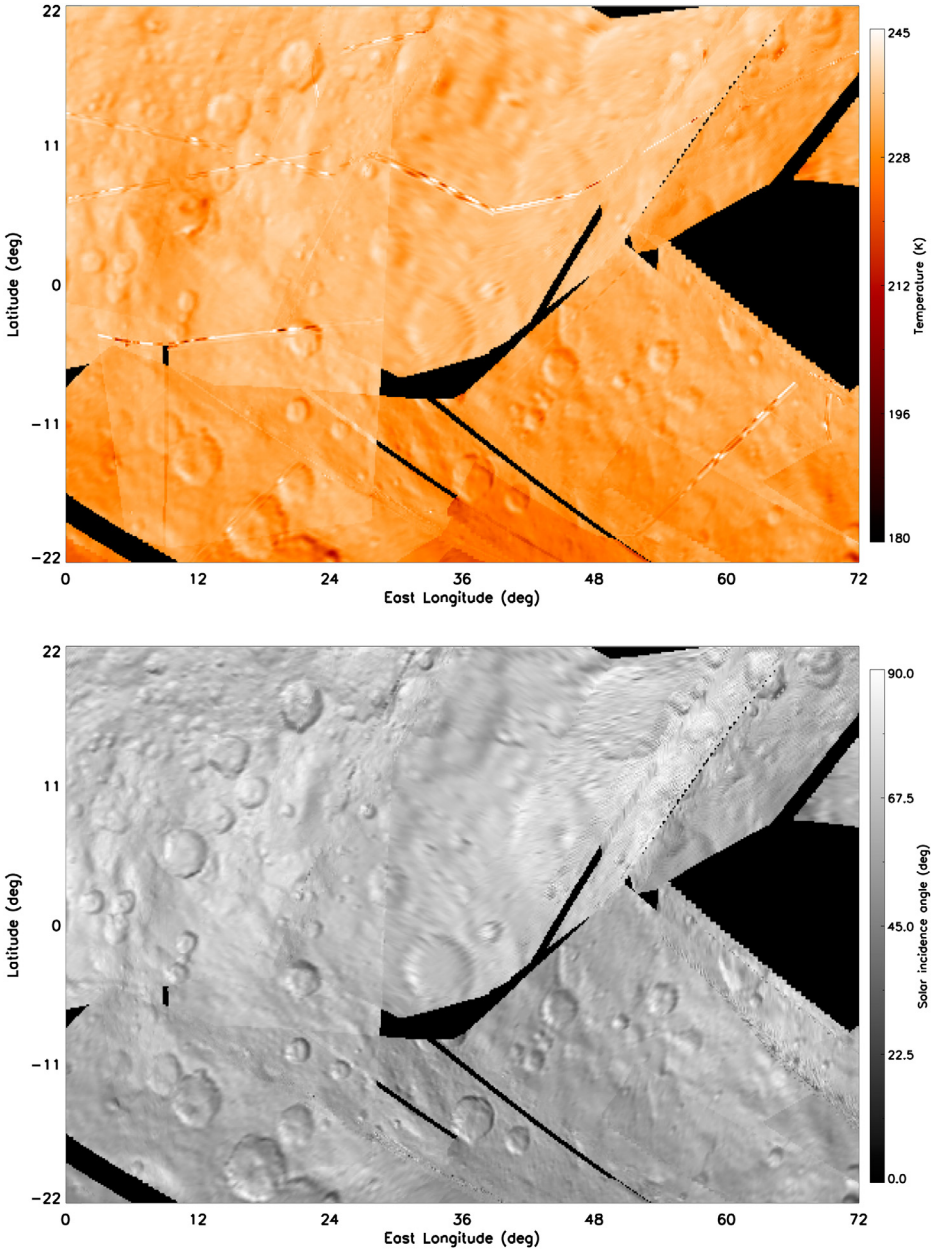

Fig. 12. a: Surface temperature map of quadrangle Ac-H-6 Haulani, derived from VIR infrared data acquired in the Survey phase at a spatial resolution of ∼1.1 km/px and in the cerean morning between. A "red temperature" color bar is adopted, such that coldest temperatures are shown in the dark red tones while warmest temperatures are whitish. The lower limit (180 K) is set by the VIR sensitivity range and the rms level of in-flight noise. In the range of local solar times analyzed here, surface temperatures are as high as 241 K. **b:** Solar incidence angle map of the same region. Surface temperatures recorded in (**a**) generally follow the local topography, in such a way that areas illuminated at large incidence angles (dark tones) are cooler than materials illuminated at small incidence angles (bright tones).(For interpretation of the references to color in this figure legend, the reader is referred to the web version of this article.)

that can be drawn from our work is still far from being able to provide definitive answers to the many open questions concerning the composition and distribution of surface materials in crater Haulani, and more generally on Ceres. Parallel work (Tosi et al., 2017, under review) focuses on VIR data obtained only in a 25° by 25° area centered on crater Haulani, applying spectral unmixing techniques to data acquired at the highest available pixel resolution (i.e., down ∼0.10 km) in order to quantify the abundances of a number of mineral species known or expected to exist at the surface, including carbonates. Since crater Haulani displays the most distinct thermal signature on the entire surface of Ceres, future work should also address a detailed thermophysical modeling of this region.

One irrefutable piece of evidence is that the Haulani event substantially changed the mineralogy of the entire quadrangle. We support the hypothesis that crater Haulani's material displaying high albedo, negative spectral slope in the visible to near infrared range, and substantial depletion in magnesium- and ammoniated-rich phyllosilicates, is the product of an intense hydrothermal process producing highly fluidized material/impact melt, which may have been favored by both the pre-existing mineralogy (e.g., water ice-rich subsurface) and the characteristics of the impact event. In specific regions within the Haulani area, the products of this impact are still so fresh and compact that they exhibit a distinct thermal signature. The young age of Haulani prevented space weathering processes to redden its surface and to crumble the compact

Please cite this article as: F. Tosi et al., Mineralogical analysis of the Ac-H-6 Haulani quadrangle of the dwarf planet Ceres, Icarus (2017), http://dx.doi.org/10.1016/j.icarus.2017.08.012

impact products into a regolith as fine as it is generally observed on Ceres.

Acknowledgments

We thank the Italian Space Agency (ASI) and NASA for supporting this work. The VIR instrument was funded and coordinated by the ASI and built by Selex ES, with the scientific leadership of the Institute for Space Astrophysics and Planetology, Italian National Institute for Astrophysics, Italy. The VIR is operated by the Institute for Space Astrophysics and Planetology, Rome, Italy. A portion of this work was carried out at the Jet Propulsion Laboratory, California Institute of Technology, under contract to NASA. Dawn data are archived in NASA's Planetary Data System; VIR spectral data may be obtained at https://sbn.psi.edu/pds/resource/dwncvir.html

References

Adams, J.B., 1974. Visible and near-infrared diffuse reflectance spectra of pyroxenes as applied to remote sensing of solid objects in the solar system. J. Geophys. Res. 79, 4829–4836. doi:10.1029/JB079i032p04829.

Archinal, B.A., A'Hearn, M.F., Bowell, E., Conrad, A., Consolmagno, G.J., Courtin, R., Fukushima, T., Hestroffer, D., Hilton, J.L., Krasinsky, G.A., Neumann, G., Oberst, J., Seidelmann, P.K., Stooke, P., Tholen, D.J., Thomas, P.C., Williams, I.P., 2011. Report of the IAU working group on cartographic coordinates and rotational elements: 2009. Cel. Mech. Dyn. Astron. 109 (2), 101–135. doi:10.1007/s10569-010-9320-4.

Ammannito, E., De Sanctis, M.C., Ciarniello, M., Frigeri, A., Carrozzo, F.G., Combe, J.-Ph., Ehlmann, B.L., Marchi, S., McSween, H.Y., Raponi, A., Toplis, M.J., Tosi, F., Castillo-Rogez, J.C., Capaccioni, F., Capria, M.T., Fonte, S., Giardino, M., Jaumann, R., Longobardo, A., Joy, S.P., Magni, G., McCord, T.B., McFadden, L.A., Palomba, E., Pieters, C.M., Polanskey, C.A., Rayman, M.D., Raymond, C.A., Schenk, P.M., Zambon, F., Russell, C.T., 2016. Distribution of phyllosilicates on the surface of Ceres. Science 353 (6303), aaf4279-1–aaf4279-5. doi:10.1126/science.aaf4279.

Bishop, J.L., Banin, A., Mancinelli, R.L., Klovstad, M.R., 2002. Detection of soluble and fixed NH_4^+ in clay minerals by DTA and IR reflectance spectroscopy: a potential tool for planetary surface exploration. Planet. Space Sci. 50 (1), 11–19. doi:10.1016/S0032-0633(01)00077-0.

Bowling, T.J., Ciesla, F.J., Marchi, S., Davison, T.M., Castillo-Rogez, J.C., De Sanctis, M.C., Raymond, C.A., Russell, C.T., 2016. Impact induced heating of Occator crater on asteroid 1 Ceres. In: 47th Lunar and Planetary Science Conference, held March 21-25, 2016 at the Woodlands, Texas, p. 2268. LPI Contribution No. 1903.

Carrozzo, F.G., Raponi, A., De Sanctis, M.C., Ammannito, E., Giardino, M., D'Aversa, E., Fonte, S., Tosi, F., 2016. Artifacts reduction in VIR/Dawn data. Rev. Sci. Instrum. 87 (12). doi:10.1063/1.4972256, id.124501.

Carrozzo, F.G., De Sanctis, M.C., Raponi, A., Ammannito, E., Castillo-Rogez, J.C., Ehlmann, B.L., Marchi, S., Stein, N., Ciarniello, M., Tosi, F., Capaccioni, F., Capria, M.T., Fonte, S., Formisano, M., Frigeri, A., Giardino, M., Longobardo, A., Magni, G., Palomba, E., Zambon, F., Raymond, C.A., Russell, C.T., 2017a. Nature, formation and distribution of carbonates on Ceres. Sci. Adv., Icarus, this issue. In press.

Carrozzo, F.G., De Sanctis, M.C., Longobardo, A., Stephan, K., Zambon, F., Ammannito, E., Ciarniello, E., Combe, J.-Ph., Frigeri, A., Palomba, E., Raponi, A., Tosi, F., Raymond, C.A., Russell, C.T., 2017b. The mineralogy of the Nawish quadrangle of Ceres. Icarus, this issue. In press.

Chapman, C.R., Salisbury, J.W., 1973. Comparisons of meteorite and asteroid spectral reflectivities. Icarus 19 (4), 507–522. doi:10.1016/0019-1035(73)90078-X.

Ciarniello, M., De Sanctis, M.C., Ammannito, E., Raponi, A., Longobardo, A., Palomba, E., Carrozzo, F.G., Tosi, F., Li, J.-Y., Schröder, S.E., Zambon, F., Frigeri, A., Fonte, S., Giardino, M., Pieters, C.M., Raymond, C.A., Russell, C.T., 2017. Spectrophotometric properties of dwarf planet Ceres from the VIR spectrometer on board the Dawn mission. Astron. Astrophys 598, A130. doi:10.1051/0004-6361/201629490.

Clark, R.N., Roush, T.L., 1984. Reflectance spectroscopy – Quantitative analysis techniques for remote sensing applications. J. Geophys. Res. 89, 6329–6340. doi:10.1029/JB089iB07p06329.

Clark, R.N., 1999. Chapter 1: spectroscopy of rocks and minerals, and principles of spectroscopy. In: Rencz, A.N. (Ed.), Manual of Remote Sensing, Volume 3, Remote Sensing For the Earth Sciences. John Wiley and Sons, New York, pp. 3–58.

Combe, J.-Ph., McCord, T.B., Tosi, F., Ammannito, E., Carrozzo, F.G., De Sanctis, M.C., Raponi, A., Byrne, S., Landis, M.E., Hughson, K.H.G., Raymond, C.A., Russell, C.T., 2016. Detection of local H_2O exposed at the surface of Ceres. Science 353 (6303). doi:10.1126/science.aaf3010, id.aaf3010.

Combe, J.-Ph., Raponi, A., Tosi, F., De Sanctis, M.C., Carrozzo, F.G., Zambon, F., Ammannito, E., Hughson, K.H.G., Nathues, A., Hoffmann, M., Platz, T., Thangjam, G., Schorghofer, N., Schröder, S.E., Byrne, S., Landis, M.E., Ruesch, O., McCord, T.B., Johnson, K.E., Singh, S.M., Raymond, C.A., Russell, C.T., 2017a. Exposed H_2O-rich areas detected on Ceres with the dawn visible and infrared mapping spectrometer. Icarus, this issue. In press.

Combe, J.-Ph., Singh, S., Johnson, K.E., McCord, T.B., De Sanctis, M.C., Ammannito, E., Carrozzo, F.G., Ciarniello, M., Frigeri, A., Raponi, A., Tosi, F., Zambon, F., Scully, J.E.C., Raymond, C.A., Russell, C.T., 2017b. The surface composition of Ceres Ezinu quadrangle analyzed by the Dawn mission. Icarus, this issue. In press.

De Sanctis, M.C., Coradini, A., Ammannito, E., Filacchione, G., Capria, M.T., Fonte, S., Magni, G., Barbis, A., Bini, A., Dami, M., Ficai-Veltroni, I., Preti, G.and the VIR Team, 2011. The VIR spectrometer. Space Sci Rev 163 (1–4), 329–369. doi:10.1007/s11214-010-9668-5.

De Sanctis, M.C., Ammannito, E., Raponi, A., Marchi, S., McCord, T.B., McSween, H.Y., Capaccioni, F., Capria, M.T., Carrozzo, F.G., Ciarniello, M., Longobardo, A., Tosi, F., Fonte, S., Formisano, M., Frigeri, A., Giardino, M., Magni, G., Palomba, E., Turrini, D., Zambon, F., Combe, J.-Ph., Feldman, W., Jaumann, R., McFadden, L.A., Pieters, C.M., Prettyman, T., Toplis, M., Raymond, C.A., Russell, C.T., 2015. Ammoniated phyllosilicates with a likely outer solar system origin on (1) Ceres. Nature 528 (7581), 241–244. doi:10.1038/nature16172.

De Sanctis, M.C., Raponi, A., Ammannito, E., Ciarniello, M., Toplis, M.J., McSween, H.Y., Castillo-Rogez, J.C., Ehlmann, B.L., Carrozzo, F.G., Marchi, S., Tosi, F., Zambon, F., Capaccioni, F., Capria, M.T., Fonte, S., Formisano, M., Frigeri, A., Giardino, M., Longobardo, A., Magni, G., Palomba, E., McFadden, L.A., Pieters, C.M., Jaumann, R., Schenk, P., Mugnuolo, R., Raymond, C.A., Russell, C.T., 2016. Bright carbonate deposits as evidence of aqueous alteration on (1) Ceres. Nature 536 (7614), 54–57. doi:10.1038/nature18290.

De Sanctis, M.C., Ammannito, E., McSween, H.Y., Raponi, A., Marchi, S., Capaccioni, F., Capria, M.T., Carrozzo, F.G., Ciarniello, M., Fonte, S., Formisano, M., Frigeri, A., Giardino, M., Longobardo, A., Magni, G., McFadden, L.A., Palomba, E., Pieters, C.M., Tosi, F., Zambon, F., Raymond, C.A., Russell, C.T., 2017a. Localized aliphatic organic material on the surface of Ceres. Science 355 (6326), 719–722. doi:10.1126/science.aaj2305.

De Sanctis, M.C., Frigeri, A., Ammannito, E., Carrozzo, F.G., Ciarniello, M., Zambon, F., Tosi, F., Raponi, A., Longobardo, A., Combe, J.-Ph., Palomba, E., Schulzeck, F., Raymond, C.A., Russell, C.T., 2017b. Ac-11-Sintana and Ac-H-12 Toharu quadrangles: Assessing the large and small scale heterogeneities of Ceres' surface. Icarus doi:10.1016/j.icarus.2017.08.014, in press.

Ehlmann, B.L., Hodyss, R.P., Bristow, T.F., Rossmann, G.R., Ammannito, E., De Sanctis, M.C., Raymond, C.A., 2017. Ambient and cold-temperature infrared spectra of ammoniated phyllosilicates and carbonaceous chondrite meteorites relevant to Ceres and other solar system bodies. Meteorit. Planet. Sci. Under review.

Frigeri, A., De Sanctis, M.C., Ammannito, E., Tosi, F., Ciarniello, M., Zambon, F., Carrozzo, F.G., Raponi, A., McCord, T.B., Raymond, C.A., Russell, C.T., 2017. The spectral parameter maps of Ceres from NASA/Dawn VIR data. Icarus, this issue. In press.

Hayne, P.O., Aharonson, O., 2015. Thermal stability of ice on Ceres with rough topography. J. Geophys. Res: Planets 120 (9), 1567–1584. doi:10.1002/2015JE004887.

Krohn, K., Jaumann, R., Stephan, K., Otto, K.A., Schmedemann, N., Wagner, R.J., Matz, K.-D., Tosi, F., Zambon, F., von der Gathen, I., Schulzeck, F., Schroder, S.E., Buczkowski, D.L., Hiesinger, H., McSween, H.Y., Pieters, C.M., Preusker, F., Roatsch, T., Raymond, C.A., Russell, C.T., Williams, D.A., 2016. Cryogenic flow features on Ceres: implications for crater-related cryovolcanism. Geophys. Res. Lett. 43 (23), 11994–12003. doi:10.1002/2016GL070370.

Krohn, K., Jaumann, R., Otto, K.A., Schulzeck, F., Neesemann, A., Nass, A., Stephan, K., Tosi, F., Wagner, R.J., Zambon, F., von der Gathen, I., Williams, D.A., Buczkowski, D.L., De Sanctis, M.C., Kersten, E., Matz, K.-D., Mest, S.C., Pieters, C.M., Preusker, F., Roatsch, T., Scully, J.E.C., Russell, C.T., Raymond, C.A., 2017. The unique geomorphology and structural geology of the Haulani crater of dwarf planet Ceres as revealed by geological mapping of equatorial quadrangle Ac-H-6 Haulani. Icarus. In press.

Li, J.-Y., McFadden, L.A., Parker, J.Wm., Young, E.F., Stern, S.A., Thomas, P.C., Russell, C.T., Sykes, M.V., 2006. Photometric analysis of 1 Ceres and surface mapping from HST observations. Icarus 182 (1), 143–160. doi:10.1016/j.icarus.2005.12.012.

Li, J.-Y., Reddy, V., Nathues, A., Le Corre, L., Izawa, M.R.M., Cloutis, E.A., Sykes, M.V., Carsenty, U., Castillo-Rogez, J.C., Hoffmann, M., Jaumann, R., Krohn, K., Mottola, S., Prettyman, T.H., Schaefer, M., Schenk, P., Schröder, S.E., Williams, D.A., Smith, D.E., Zuber, M.T., Konopliv, A.S., Park, R.S., Raymond, C.A., Russell, C.T., 2016. Surface albedo and spectral variability of Ceres. Astrophys. J. Lett. 817 (2). doi:10.3847/2041-8205/817/2/L22, article id. L22.

Longobardo, A., Palomba, E., Carrozzo, F.G., Galiano, A., De Sanctis, M.C., Stephan, K., Tosi, F., Raponi, A., Ciarniello, M., Zambon, F., Frigeri, A., Ammannito, E., Capria, M.T., Raymond, C.A., Russell, C.T., 2017. Mineralogy of the Occator quadrangle. Icarus, this issue. In press.

McCord, T.B., Li, J.-Y., Combe, J.-Ph., McSween, H.Y., Jaumann, R., Reddy, V., Tosi, F., Williams, D.A., Blewett, D.T., Turrini, D., Palomba, E., Pieters, C.M., De Sanctis, M.C., Ammannito, E., Capria, M.T., Le Corre, L., Longobardo, A., Nathues, A., Mittlefehldt, D.W., Schröder, S.E., Hiesinger, H., Beck, A.W., Capaccioni, F., Carsenty, U., Keller, H.U., Denevi, B.W., Sunshine, J.M., Raymond, C.A., Russell, C.T., 2012. Dark material on Vesta from the infall of carbonaceous volatile-rich material. Nature 491 (7422), 83–86. doi:10.1038/nature11561.

Nathues, A., Hoffmann, M., Platz, T., Thangjam, G.S., Cloutis, E.A., Reddy, V., Le Corre, L., Li, J.-Y., Mengel, K., Rivkin, A., Applin, D.M., Schaefer, M., Christensen, U., Sierks, H., Ripken, J., Schmidt, B.E., Hiesinger, H., Sykes, M.V., Sizemore, H.G., Preusker, F., Russell, C.T., 2016. FC colour images of dwarf planet Ceres reveal a complicated geological history. Planet. Space Sci. 134, 122–127. doi:10.1016/j.pss.2016.10.017.

Nathues, A., Platz, T., Thangjam, G., Hoffmann, M., Mengel, K., Cloutis, E.A., Le Corre, L., Reddy, V., Kallisch, J., Crown, D.A., 2017. Evolution of Occator crater on (1) Ceres. Astron. J. 153 (3). doi:10.3847/1538-3881/153/3/112, article id. 112.

Palomba, E., Longobardo, A., De Sanctis, M.C., Carrozzo, F.G., Galiano, A., Zambon, F., Raponi, A., Ciarniello, M., Stephan, K., Williams, D.A., Ammannito, E., Capria, M.T., Fonte, S., Giardino, M., Tosi, F., Raymond, C.A., Russell, C.T., 2017a. Mineralogical mapping of the Kerwan quadrangle on Ceres. Icarus doi:10.1016/j.icarus.2017.07.021, Submitted for publication.

Palomba, E., Longobardo, A., De Sanctis, M.C., Stein, N.T., Ehlmann, B., Galiano, A., Raponi, A., Ciarniello, M., Ammannito, E., Cloutis, E., Carrozzo, F.G., Capria, M.T., Stephan, K., Zambon, F., Tosi, F., Raymond, C.A., Russell, C.T., 2017b. Compositional differences among bright spots on the Ceres surface. Icarus, this issue. In press.

Park, R.S., Konopliv, A.S., Bills, B.G., Rambaux, N., Castillo-Rogez, J.C., Raymond, C.A., Vaughan, A.T., Ermakov, A.I., Zuber, M.T., Fu, R.R., Toplis, M.J., Russell, C.T., Nathues, A., Preusker, F., 2016. A partially differentiated interior for (1) Ceres deduced from its gravity field and shape. Nature 537 (7621), 515–517. doi:10.1038/nature18955.

Pieters, C.M., Staid, M.I., Fischer, E.M., Tompkins, S., He, G., 1994. A sharper view of impact craters from Clementine data. Science 266 (5192), 1844–1848. doi:10.1126/science.266.5192.1844.

Platz, T., Nathues, A., Schorghofer, N., Preusker, F., Mazarico, E., Schröder, S.E., Byrne, S., Kneissl, T., Schmedemann, N., Combe, J.-Ph., Schäfer, M., Thangjam, G.S., Hoffmann, M., Gutierrez-Marques, P., Landis, M.E., Dietrich, W., Ripken, J., Matz, K.-D., Russell, C.T., 2016. Surface water-ice deposits in the northern shadowed regions of Ceres. Nat. Astron 1. doi:10.1038/s41550-016-0007, id. 0007.

Platz, T., Nathues, A., Sizemore, H.G., Crown, D.A., Hoffmann, M., Schäfer, M., Schmedemann, N., Kneissl, T., Neesemann, A., Mest, S.C., Buczkowski, D.L., Ruesch, O., Hughson, K.H.G., Nass, A., Williams, D.A., Preusker, F., 2017. Geologic mapping of the Ac-H-10 Rongo quadrangle of Ceres. Icarus. doi:10.1016/j.icarus.2017.08.001.

Prettyman, T.H., Yamashita, N., Toplis, M.J., McSween, H.Y., Schörghofer, N., Marchi, S., Feldman, W.C., Castillo-Rogez, J., Forni, O., Lawrence, D.J., Ammannito, E., Ehlmann, B.L., Sizemore, H.G., Joy, S.P., Polanskey, C.A., Rayman, M.D., Raymond, C.A., Russell, C.T., 2017. Extensive water ice within Ceres' aqueously altered regolith: Evidence from nuclear spectroscopy. Science 355 (6320), 55–59. doi:10.1126/science.aah6765.

Preusker, F., Scholten, F., Matz, K.-D., Elgner, S., Jaumann, R., Roatsch, T., Joy, S.P., Polanskey, C.A., Raymond, C.A., Russell, C.T., 2016. 47th Lunar and Planetary Science Conference, The Woodlands, Texas, 21-25 March 2016, p. 1954. LPI Contribution No. 1903 ADS Bibcode: 2016LPI....47.1954P.

Raponi, A., Carrozzo, F.G., Zambon, F., De Sanctis, M.C., Ciarniello, M., Frigeri, A., Ammannito, E., Tosi, F., Combe, J.-Ph., Longobardo, A., Palomba, E., Pieters, C.M., Raymond, C.A., Russell, C.T., 2017. Mineralogical mapping of Coniraya quadrangle of the dwarf planet Ceres. Icarus, this issue. In press.

Raymond, C.A., Roatsch, T., 2015. Ceres coordinate system description. https://sbn.psi.edu/pds/resource/ceres_coord_sys_151014.pdf.

Rivkin, A.S., Volquardsen, E.L., Clark, B.E., 2006. The surface composition of Ceres: discovery of carbonates and iron-rich clays. Icarus 185 (2), 563–567. doi:10.1016/j.icarus.2006.08.022.

Roatsch, T., Kersten, E., Matz, K.-D., Preusker, F., Scholten, F., Jaumann, R., Raymond, C.A., Russell, C.T., 2016a. Ceres survey atlas derived from Dawn Framing Camera images. Planet. Space Sci. 121, 115–120. doi:10.1016/j.pss.2015.12.005.

Roatsch, T., Kersten, E., Matz, K.-D., Preusker, F., Scholten, F., Jaumann, R., Raymond, C.A., Russell, C.T., 2016b. High-resolution ceres high altitude mapping orbit atlas derived from Dawn Framing Camera images. Planet. Space Sci. 129, 103–107. doi:10.1016/j.pss.2016.05.011.

Russell, C.T., Raymond, C.A., Ammannito, E., Buczkowski, D.L., De Sanctis, M.C., Hiesinger, H., Jaumann, R., Konopliv, A.S., McSween, H.Y., Nathues, A., Park, R.S., Pieters, C.M., Prettyman, T.H., McCord, T.B., McFadden, L.A., Mottola, S., Zuber, M.T., Joy, S.P., Polanskey, C., Rayman, M.D., Castillo-Rogez, J.C., Chi, P.J., Combe, J.-Ph., Ermakov, A., Fu, R.R., Hoffmann, M., Jia, Y.D., King, S.D., Lawrence, D.J., Li, J.-Y., Marchi, S., Preusker, F., Roatsch, T., Ruesch, O., Schenk, P., Villarreal, M.N., Yamashita, N., 2016. Dawn arrives at Ceres: exploration of a small, volatile-rich world. Science 353 (6303), 1008–1010. doi:10.1126/science.aaf4219.

Schmedemann, N., Kneissl, T., Neesemann, A., Stephan, K., Jaumann, R., Krohn, K., Michael, G.G., Matz, K.-D., Otto, K.A., Raymond, C.A., Russell, C.T., 2016. Timing of optical maturation of recently exposed material on Ceres. Geophys. Res. Lett. 43 (23), 11,987–11,993. doi:10.1002/2016GL071143.

Schmidt, B.E., Hughson, K.H.G., Chilton, H.T., Scully, J.E.C., Platz, T., Nathues, A., Sizemore, H., Bland, M.T., Byrne, S., Marchi, S., O'Brien, D.P., Schorghofer, N., Hiesinger, H., Jaumann, R., Pasckert, J.-H., Lawrence, J.D., Buczkowski, D.L., Castillo-Rogez, J.C., Sykes, M.V., Schenk, P.M., De Sanctis, M.C., Mitri, G., Formisano, M., Li, J.-Y., Reddy, V., LeCorre, L., Russell, C.T., Raymond, C.A., 2017. Geomorphological evidence for ground ice on dwarf planet Ceres. Nat. Geosci. 10 (5), 338–343. doi:10.1038/ngeo2936.

Schröder, S.E., Mottola, S., Carsenty, U., Ciarniello, M., Jaumann, R., Li, J.-Y., Longobardo, A., Palmer, E., Pieters, C.M., Preusker, F.C., Raymond, C.A., Russell, C.T., 2017. Resolved spectrophotometric properties of the Ceres surface from Dawn Framing Camera images. Icarus 288, 201–225. doi:10.1016/j.icarus.2017.01.026.

Schulzeck, F., Krohn, K., van der Gathen, I., Schmedemann, N., Stephan, K., Jaumann, R., Williams, D.A., Buczkowski, D.L., Mest, S.C., Scully, J.E.C., Kersten, E., Matz, K.-D., Nass, A., Preusker, F., Roatsch, T., Raymond, C.A., Russell, C.T., 2017. Geologic mapping of the Ac-H-11 Sintana quadrangle: assessing diverse crater morphologies. Icarus Submitted for publication.

Shepard, M.K., Helfenstein, P., 2007. A test of the Hapke photometric model. J. Geophys. Res 112 (E3). doi:10.1029/2005JE002625, CiteID E03001.

Sierks, H., Keller, H.U., Jaumann, R., Michalik, H., Behnke, T., Bubenhagen, F., Büttner, I., Carsenty, U., Christensen, U., Enge, R., Fiethe, B., Gutiérrez-Marqués, P., Hartwig, H., Krüger, H., Kühne, W., Maue, T., Mottola, S., Nathues, A., Reiche, K.-U., Richards, M.L., Roatsch, T., Schröder, S.E., Szemerey, I., Tschentscher, M., 2011. The Dawn Framing Camera. Space Sci Rev 163 (1–4), 263–327. doi:10.1007/s11214-011-9745-4.

Singh, S., Combe, J.-Ph., McFadden, L.A., McCord, T.B., Johnson, K.E., Hughson, K.H.G., Zambon, F., Ciarniello, M., Carrozzo, F.G., Ammannito, E., De Sanctis, M.C., Ruesch, O., Stephan, K., Tosi, F., Longobardo, A., Raymond, C.A., Russell, C.T., 2017. Mineralogy mapping of the Ac-H-5 Fejokoo quadrangle of Ceres. Icarus, this issue. In press.

Sizemore, H.G., Platz, T., Schorghofer, N., Prettyman, T.H., De Sanctis, M.C., Crown, D.A., Schmedemann, N., Neesemann, A., Kneissl, T., Marchi, S., Schenk, P.M., Bland, M.T., Schmidt, B.H., Hughson, K.H.G., Tosi, F., Zambon, F., Mest, S.C., Yingst, R.A., Williams, D.A., Russell, C.T., Raymond, C.A., 2017. Pitted terrains on (1) Ceres and implications for shallow subsurface volatile distribution. Geophys. Res. Lett. 44 (13), 6570–6578. doi:10.1002/2017GL073970.

Stephan, K., Jaumann, R., Krohn, K., Schmedemann, N., Zambon, F., Tosi, F., Carrozzo, F.G., McFadden, L.A., Otto, K., De Sanctis, M.C., Ammannito, E., Matz, K.-D., Roatsch, T., Preusker, F., Raymond, C.A., Russell, C.T., 2017a. An investigation of the bluish material on Ceres. Geophys. Res. Lett. 44 (4), 1660–1668. doi:10.1002/2016GL071652.

Stephan, K., Jaumann, R., Zambon, F., Carrozzo, F.G., De Sanctis, M.C., Tosi, F., Longobardo, A., Palomba, E., Ammannito, E., McFadden, L.A., Krohn, K., Williams, D.A., Raponi, A., Ciarniello, M., Combe, J.-Ph., Frigeri, A., Roatsch, T., Matz, K.-D., Preusker, F., Raymond, C.A., Russell, C.T., 2017b. Spectral investigation of quadrangle Ac-H-3 of the dwarf planet Ceres – The region of impact crater Dantu. Icarus (this issue) doi:10.1016/j.icarus.2017.07.019, in press.

Titus, T.N., 2015. Ceres: predictions for near-surface water ice stability and implications for plume generating processes. Geophys. Res. Lett. 42 (7), 2130–2136. doi:10.1002/2015GL063240.

Tosi, F., Capria, M.T., De Sanctis, M.C., Combe, J.-Ph., Zambon, F., Nathues, A., Schröder, S.E., Li, J.-Y., Palomba, E., Longobardo, A., Blewett, D.T., Denevi, B.W., Palmer, E., Capaccioni, F., Ammannito, E., Titus, T.M., Mittlefehldt, D.W., Sunshine, J.M., Russell, C.T., Raymond, C.A. and the Dawn/VIR Team, 2014. Thermal measurements of dark and bright surface features on Vesta as derived from Dawn/VIR. Icarus 240, 36–57. doi:10.1016/j.icarus.2014.03.017.

Tosi, F., De Sanctis, M.C., Zambon, F., Ammannito, E., Capria, M.T., Carrozzo, F.G., Li, J.-Y., Longobardo, A., Mottola, S., Palomba, E., Raponi, A., Raymond, C.A., Russell, C.T., 2015a. Preliminary temperature maps of dwarf planet Ceres as derived by Dawn/VIR. In: European Planetary Science Congress 2015 27 September - 2 October 2015, Nantes (France). ADS Bibcode: 2015EPSC...10..281T.

Tosi, F., Frigeri, A., Combe, J.-Ph., Zambon, F., De Sanctis, M.C., Ammannito, E., Longobardo, A., Hoffmann, M., Nathues, A., Garry, W.B., Blewett, D.T., Pieters, C.M., Palomba, E., Stephan, K., McFadden, L.A., McSween, H.Y., Russell, C.T., Raymond, C.A. the Dawn Science Team, 2015b. Mineralogical analysis of the Oppia quadrangle of asteroid (4) Vesta: evidence for occurrence of moderate-reflectance hydrated minerals. Icarus 259, 129–149. doi:10.1016/j.icarus.2015.05.018.

Tosi, F., Carrozzo, F.G., Raponi, A., De Sanctis, M.C., Zambon, F., Ciarniello, M., Thangjam, G., Nathues, A., Hoffmann, M., Ammannito, E., Krohn, K., Longobardo, A., Palomba, E., Pieters, C.M., Stephan, K., Raymond, C.A., Russell, C.T., 2017. Mineralogy of crater Haulani on Ceres. Meteorit. Planet. Sci. Under review.

Zambon, F., Tosi, F., Carli, C., De Sanctis, M.C., Blewett, D.T., Palomba, E., Longobardo, A., Frigeri, A., Ammannito, E., Russell, C.T., Raymond, C.A., 2016. Lithologic variation within bright material on Vesta revealed by linear spectral unmixing. Icarus 272, 16–31. doi:10.1016/j.icarus.2016.01.009.

Zambon, F., Raponi, A., Tosi, F., De Sanctis, M.C., McFadden, L.A., Carrozzo, F.G., Longobardo, A., Ciarniello, M., Krohn, K., Stephan, K., Palomba, E., Pieters, C.M., Ammannito, E., Russell, C.T., Raymond, C.A., 2017a. Spectral analysis of Ahuna mons from Dawn mission's visible-infrared spectrometer. Geophys. Res. Lett. 44 (1), 97–104. doi:10.1002/2016GL071303.

Zambon, F., Carrozzo, F.G., Tosi, F., Ciarniello, M., Combe, J.-Ph., Frigeri, A., De Sanctis, M.C., Hoffmann, M., Longobardo, A., Nathues, A., Stephan, K., Raponi, A., Thangjam, G., Ammannito, E., Krohn, K., McFadden, L.A., Palomba, E., Raymond, C.A., Russell, C.T. the Dawn Science Team, 2017b. Spectral analysis of the quadrangle Ac-H-10 Rongo on Ceres. Icarus, this issue. In press.

Please cite this article as: F. Tosi et al., Mineralogical analysis of the Ac-H-6 Haulani quadrangle of the dwarf planet Ceres, Icarus (2017), http://dx.doi.org/10.1016/j.icarus.2017.08.012